Flame structure analysis and composition space modeling of thermodiffusively unstable premixed hydrogen flames — Part I: Atmospheric pressure

Xu Wen[a,*], Thorsten Zirwes[b,c], Arne Scholtissek[a], Hannes Böttler[a], Feichi Zhang[c], Henning Bockhorn[c], Christian Hasse[a]

[a]*Simulation of Reactive Thermo-Fluid Systems, TU Darmstadt, Otto-Berndt-Straße 2, 64287 Darmstadt, Germany*
[b]*Steinbuch Centre for Computing, Karlsruhe Institute of Technology, Hermann-von-Helmholtz-Platz 1, 76344 Eggenstein-Leopoldshafen, Germany*
[c]*Engler-Bunte-Institute, Karlsruhe Institute of Technology, Engler-Bunte-Ring 7, 76131 Karlsruhe, Germany*

Abstract

This work focuses on flame structure analysis and composition space modeling of a multidimensional premixed hydrogen flame transitioning from a laminar stable condition to a thermodiffusively unstable state. Specifically, *budget* and *a priori* analyses are conducted based on a detailed chemistry simulation of a 2D expanding, thermodiffusively unstable hydrogen flame, and the recurring issues for modeling differential diffusion, the strain rate and curvature in the thermodiffusively unstable flame are addressed in a single newly proposed flamelet tabulation method. The model is based on recently developed self-contained strained-curved premixed flamelet equations in composition space (Scholtissek et al., 2019, CNF), which inherently incorporate the interactions among differential diffusion, the strain rate and curvature. The validity of the newly proposed flamelet tabulation method is evaluated based on the representative strongly strained-curved flamelets extracted from the reference simulation, featuring wide ranges of strain rates and curvatures. The advance realized in the proposed flamelet model is confirmed by comparing it with a conventional flamelet tabulation method. Through the *budget* analysis, the effects of curvature on the diffusion along the flame front (i.e., tangential diffusion) are quantified. Through the *a priori* analysis, the suitability of the proposed flamelet tabulation method in predicting differential diffusion is confirmed. For the prediction of the strain rate and curvature, it is found that introducing the strain rate and curvature themselves as the trajectory variables does not necessarily improve the prediction accuracy in the reaction zone, compared to the flamelet model based on the 1D freely-

---

*Corresponding author:
Email address:* wen@stfs.tu-darmstadt.de (Xu Wen)

propagating premixed flame with differential diffusion. To remedy this, the trajectory variables that can characterize the flame structure's internal response to the strain rate and curvature are identified. The results show that the thermo-chemical variables in the thermodiffusively unstable flame at atmospheric pressure can be accurately predicted by the newly introduced trajectory variables based on the 1D strained-curved flamelet equations.

1. Introduction

Hydrogen (H_2) is drawing renewed and rapidly growing attention in Europe and around the world. One of the most important advantages of hydrogen usage is that its thermochemical conversion does not lead to emissions of the greenhouse gas CO_2. For hydrogen combustion, the most challenging issues are the augmented effects of differential diffusion and the induced intrinsic instability, which can substantially change flame dynamics and heat release rates, and lead to safety problems. The intrinsic instability of hydrogen combustion comprises two mechanisms [1, 2]: (i) the hydrodynamic instability due to the density jump across the flame front, and (ii) the thermodiffusive instability due to the disparity between the heat flux leaving the reaction zone and the mass flux entering the reaction zone, which is related to the effective Lewis number of the unburnt mixture. In a thermodiffusively unstable flame, the flame front is strongly corrugated over different length scales. The distributions of the thermo-chemical variables in such flames are closely related to the strain rate and curvature of the flame front, including both positive and negative strain rates and curvatures [3–8]. The fact that positive and negative strain rates and curvatures span wide ranges challenges the state-of-the-art numerical methods.

This work mainly focuses on the flamelet tabulation methods [9, 10] used to reproduce the differential diffusion, strain rate and curvature effects in the thermodiffusively unstable hydrogen flame. In the flamelet model, one-dimensional (1D) flames are calculated *a priori*, and the obtained thermo-chemical quantities are tabulated as a flamelet table, which will be accessed by the flow solver. Characteristics of the flame structure can be represented by a 1D canonical flamelet configuration in physical space, such as the counterflow flame, the tubular flame, etc. The tubular flame has been adopted in previous flamelet tabulation methods to characterize the curvature effects [11, 12]. However, the full range of the physical parameters in a combustion system may not be

covered by the canonical flamelet configurations in physical space. For example, the negative strain rate is difficult to capture by the 1D counterflow flame due to the instability problem [13], and only a limited range of curvatures can be captured by the 1D tubular flame due to the restricted nozzle radius. In the thermodiffusively unstable hydrogen flame, both the negative and positive strain rate and the curvature span wide ranges at the flame cusps. To remedy the limitations of the flamelet configurations in physical space, Scholtissek et al. [14, 15] developed strained-curved flamelet (SCF) equations in a self-contained composition space, in which the strain rate and curvature can be prescribed as external parameters by solving an additional equation for the progress variable gradient. The capability of the developed flamelet in representing wide ranges of strain rates and curvatures has been demonstrated in our previous work [16], compared to the flamelet model based on the canonical configuration in physical space. However, the developed premixed flamelet equations in composition space have not been implemented in a flamelet tabulation method to evaluate whether the strong strain rate and curvature can be reproduced, which is the main purpose of this work.

Differential diffusion is still a recurring issue for flamelet modeling due to its physical complexity, although many works have addressed this topic for either turbulent flames or laminar flames. Representative works on flamelet modeling of differential diffusion are reviewed next. Pitsch and Peters [17] proposed a consistent flamelet formulation to consider differential diffusion in non-premixed flames. The differential diffusion was described by the mixture fraction transport equation with an arbitrary diffusion coefficient and appropriate boundary conditions. The suitability of the flamelet formulation was evaluated, but it has not actually been used for flamelet tabulation. Swart et al. [18] proposed that differential diffusion could be included in the tabulation method of flamelet-generated manifolds [19] for laminar premixed flames. The flamelet solutions were obtained from the 1D laminar stretched premixed flames, while differential diffusion was considered by a second controlling variable related to the elemental mass fraction of C and H. Donini et al. [20] further modified the tabulation method of Swart et al. [18]. The source terms introduced due to differential diffusion were incorporated in the governing equations of the trajectory variables, and the Bilger mixture fraction [21] was introduced to characterize the redistribution of the species due to differential diffusion. For laminar non-premixed flames, Verhoeven et al. [22, 23] considered differential diffusion in the transport equation of the reaction progress variable, while the Lewis number for the other trajectory variable, mixture fraction, was assumed to be unity.

Regele et al. [24] proposed a two-equation model (for the mixture fraction and reaction progress variable) to consider differential diffusion in the laminar premixed flame. In contrast to the work of Verhoeven et al. [22, 23], differential diffusion was only considered in the transport equation of the mixture fraction with an additional source term, while it was neglected in the reaction progress variable transport equation. The mixture fraction equation was derived based on the unity Lewis number assumption for all species except for the fuel. In the context of large-eddy simulation, Mercier et al. [25] proposed a flamelet tabulation method in which differential diffusion in the reaction progress variable equation was consistently considered, while the mixture fraction was assumed to be only a function of the progress variable and equivalence ratio of the fresh gas.

In the case of flamelet modeling of *strained flames*, progress has been made in recent years. Kolla and Swaminathan [26] proposed a strained flamelet model for turbulent premixed flames, in which the scalar dissipation rate of the reaction progress variable was used to represent the strain rate. The 1D reactants-to-products (R2P) flamelet configuration was selected to represent strain rate effects. Knudsen et al. [27] also proposed a strained flamelet model for turbulent premixed flames in which the mass fraction of H radical was chosen to capture strain effects. The back-to-back (B2B) flamelet configuration was selected to characterize the flame structure's internal response to the strain rate. Trisjono et al. [28] further modified the model developed by Knudsen et al. [27] by selecting the mass fraction of H_2 to characterize the strain rate's effects on the flame structure for the particular flame studied. Again, the flamelet solutions were obtained based on the 1D B2B flamelet configuration in physical space. With the H_2 mass fraction as the flamelet coordinate and the 1D R2P as the flamelet configuration, we also evaluated the performance of the strained flamelet model through *prior* analyses using instantaneous Raman/Rayleigh datasets [29]. In contrast to previous works where the strain rate is represented by the canonical flamelet configuration, van Oijen et al. [30] obtained the flamelet solutions from the flamelet equations with the flame stretch (strain rate or curvature) as an additional parameter. To access the flamelet table, the flame stretch was mapped to the flamelet coordinate of the OH mass fraction.

With regard to flamelet modeling of *curved flames*, different approaches have been proposed in previous works. Xu et al. [31] proposed a consistent flamelet formulation to consider the curvature effects in a reacting char particle. The curvature effects are demonstrated to be significant, especially in the wake region downstream of the particle, by comparing the flamelet equations with or without the curvature terms. However, the consistent flamelet formulation has not been used for

flamelet tabulation by introducing proper trajectory variables. Xuan et al. [11] investigated the effects of curvature on the species transport in diffusion flames. A consistent flamelet formulation was derived which considered differential diffusion and curvature effects, and the flamelet tabulation was conducted by introducing curvature as an additional trajectory variable in the flamelet table apart from the mixture fraction and the scalar dissipation rate. The authors argued that significant improvements can be obtained if the curvature effects are considered, even though non-negligible tangential diffusion exists. Schlup and Blanquart [32] extended the flamelet equations proposed by Regele et al. [24] by further considering differential diffusion and the thermal diffusion of multiple species. These were used to predict the curvature effects due to differential diffusion using the flamelet tabulation method. The flamelet solutions were tabulated as a function of the reaction progress variable and mixture fraction. Recently, Göktolga et al. [12] adopted a so-called multistage flamelet tabulation method to reproduce the curvature-differential diffusion interactions in a turbulent auto-igniting non-premixed flame. The flamelet solutions were obtained from an opposed tubular flow configuration for various curvatures at a constant strain rate. Unlike the work by Xuan et al. [11] where the curvature itself is used to parameterize the flamelet table, Göktolga et al. [12] proposed using a normalized mixture fraction as the trajectory variable, with its diffusion coefficient equal to that of H_2.

Although significant progress has been made in flamelet modeling of differential diffusion, the strain rate and curvature, the coupled effects have not been comprehensively considered together. The purpose of this work is to develop a consistent flamelet model that can accurately reproduce all the effects of differential diffusion, the strain rate and curvature. Considering the limitations of the flamelet configuration in physical space in representing the strain rate and curvature, a recently developed self-contained composition space method for solving an arbitrary combination of the strain rate and curvature [14, 15] is used to generate flamelet solutions, taking into account differential diffusion. Among other things, this method has two significant advantages over the flamelet equations in physical space. On the one hand, differential diffusion, the strain rate and curvature can be considered with a single set of flamelet equations, independently of the flamelet configuration in physical space. On the other hand, a significantly extended range of strain rates and curvatures can be obtained with the formulated flamelet equations in composition space [16], which addresses the limitations of the flamelet configuration in physical space related to the burner geometry, restrainment of the stagnation flame, etc. The latter advantage is particularly important

for predicting the thermodiffusively unstable flame, in which both the negative and positive strain rates and curvatures span wide ranges. The suitability of the new flamelet tabulation method is systematically evaluated through *a priori* analyses. Moreover, the first flamelet analysis of the thermo-chemical state and the reaction zone structure of the thermodiffusively unstable premixed hydrogen flame is conducted, together with a *budget analysis* of the generalized premixed flamelet equations in composition space.

In the *a priori* analysis, the trajectory variables are calculated from the reference results, e.g., 1D detailed chemistry solutions, DNS results, etc. Then, the tabulated values are compared to the corresponding reference results. In the *budget analysis*, the budget terms in the generalized flamelet equations, including the transient, convection, normal diffusion, tangential diffusion, reaction rate, etc., are calculated from the reference results. Then, the budget terms are compared with each other to identify the importance of different physical processes.

The remainder of the paper is organized as follows: The numerical implementations for the thermodiffusively unstable flame are described in Section 2. Section 3 presents the modeling methods. Section 4 outlines the results and discussions of the reference simulation, and Section 5 presents the verfication of the flamelet models. The last section summarizes the findings of this work.

2. Numerical implementations

In this work, a reference simulation for the thermodiffusively unstable premixed hydrogen flame is conducted to evaluate the performance of the different flamelet tabulation methods, described in the next section. As shown in Fig. 1, the adopted computational domain is 2D as in the previous works [3, 5, 7, 8, 33]. Specifically, it is a rotationally symmetrical wedge with a radius of $0.08\,\mathrm{m}$ and an angle of $5°$ in the Cartesian coordinates, see Fig. 1a. The center of the domain, with a radius of 0.01 m, is initialized with the burnt products of H_2/air at the equivalence ratio of 0.4, while the other parts of the domain are initialized with an unburnt mixture of H_2/air at the same equivalence ratio and a temperature of 300 K. With such a lean H_2/air mixture, thermodiffusive instabilities are significant, as already demonstrated by Berger et al. [8] for the same equivalence ratio. Berger et al. [8] reported that as the equivalence ratio of the unburnt H_2/air mixture increases from 0.4 to 0.65, the presence of finger structures in the thermodiffusively unstable flame becomes rather weak, and a rather flat flame can be observed. Thus, the extremely lean premixed hydrogen flame
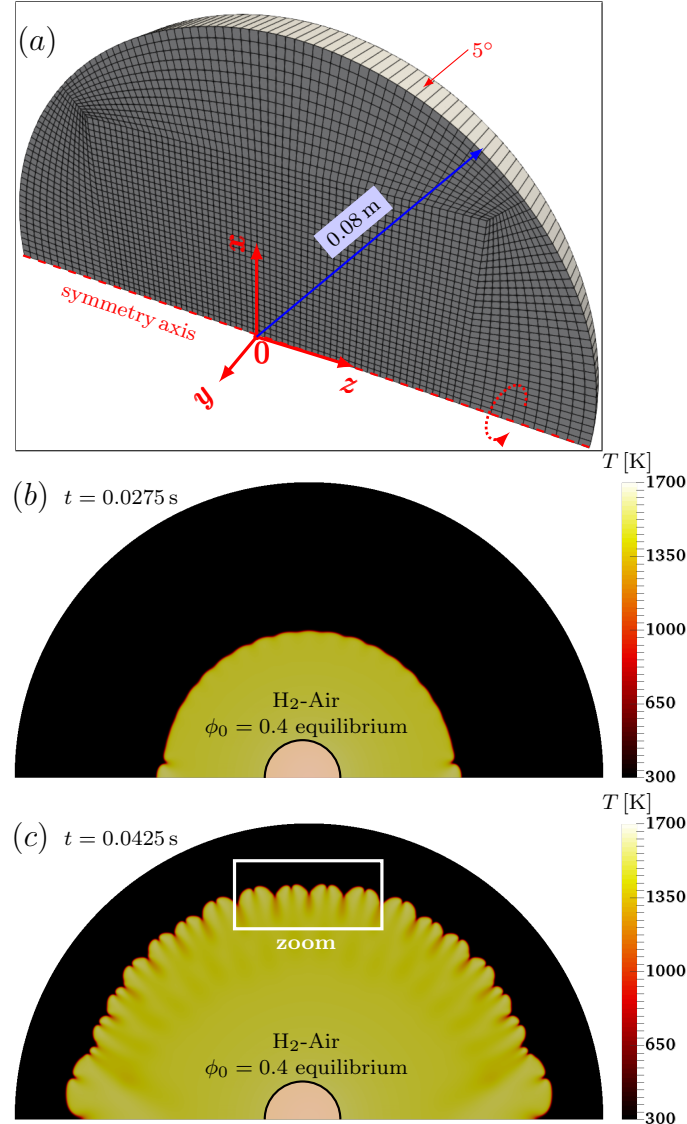
Fig. 1. (a) Computational domain with grid setup superimposed (only 3240 cells are shown for clarity), and the instantaneous distributions of the temperature for the expanding premixed hydrogen flame at (b) the early state ($t = 0.0275\,\text{s}$), and (c) the thermodiffusively unstable state ($t = 0.0425\,\text{s}$). The initial region in the center is indicated. The zoomed region in (c) will be investigated in detail in Section 4.

with significant thermodiffusive instabilities is simulated in this work to challenge the proposed flamelet tabulation method. Instantaneous distributions of the temperature at the early laminar state and the latter thermodiffusively unstable state are shown in Figs. 1b and 1c, respectively, to illustrate the expansion of the premixed flame. In the x and z directions, 4500 and 7200 grid points are set with local refinement, see Fig. 1a for the mesh setup. For the studied operating conditions, the thermal flame thickness calculated according to the temperature gradient is 0.641 mm, while

the largest mesh size is 0.032 mm, resulting in at least 20 grid points to resolve the laminar flame thickness. For the same operating conditions, Berger et al. [8] adopted 10 grid points to resolve the laminar flame thickness, and confirmed that the adopted mesh resolution is sufficient.

The boundaries in the flame propagation direction are superimposed with the zero-gradient boundary condition for both velocity and scalars, while the two rotational symmetry boundaries in the y direction are superimposed with the wedge boundary condition [34] for both velocity and scalars. Note that some perturbations can be found near the $x = 0$ boundary with the employed boundary conditions. However, such perturbations cannot be totally removed by using the other boundary conditions. As the selected region for model evaluation is in the middle of the computational domain, we believe the adopted boundary conditions will not change the findings reported in this work.

In the reference simulation, the governing equations for the species mass fractions and sensible enthalpy in their fully compressible formulation are solved using a solver [35–39] developed based on the open-source code OpenFOAM [40]. In order to calculate the detailed molecular diffusion coefficients and the finite reaction rates from the detailed chemistry mechanism, the flow solver is coupled with the open-source library Cantera [41]. The details of the governing equations are described in our previous works [38, 39], and are not repeated here for simplicity. The diffusion flux is calculated with the mixture-averaged approach (detailed molecular diffusion with Hirschfelder-Curtiss approximation [42]), and the chemical reaction mechanism developed by Varga et al. [43] (12 species and 29 elementary reactions) is utilized in the reference simulation. A second-order backward scheme is used for the time discretization, while a cubic scheme is employed for the spatial discretization. The time-step is calculated according to the Courant number, which is set to be 0.15 to ensure the stability of the simulation.

3. Modeling approach

In this section, the premixed flamelet equations in composition space are presented, together with the different tabulation methods for the differential diffusion, strain rate and curvature.

3.1. Premixed flamelet equations in composition space

The premixed flamelet equations with the strain rate and curvature in composition space are derived through a coordinate transformation of governing equations in physical space. The derivation process for the species mass fraction Y_i and temperature T without tangential diffusion is

8

reported in Scholtissek et al. [14]. In this work, the generalized premixed flamelet equations are derived, in which the tangential diffusion terms are included for *budget analysis*. The detailed derivation process is provided in the Supplementary Material. The resulting generalized premixed flamelet equations for species mass fraction and temperature are written as,

$$
\rho \underbrace{\frac{\partial Y_i}{\partial \tau}}_{\Lambda_{\text{tran}}^{Y_i}} = \underbrace{-g_c \frac{\partial}{\partial Y_{PV}} \left(g_c \rho Y_i \widetilde{V}_i \right)}_{\Lambda_{\text{diff}}^{Y_i}} + \underbrace{g_c \frac{\partial}{\partial Y_{PV}} \left(g_c \rho Y_{PV} \widetilde{V}_c \right) \frac{\partial Y_i}{\partial Y_{PV}}}_{\Lambda_{\text{conv}}^{Y_i}} + \underbrace{\kappa_c \left(g_c \rho Y_i \widetilde{V}_i - g_c \rho Y_{PV} \widetilde{V}_c \frac{\partial Y_i}{\partial Y_{PV}} \right)}_{\Lambda_{\text{curv}}^{Y_i}}
$$
$$
+ \underbrace{\left[-\nabla \cdot \left(\rho Y_i \overrightarrow{V}_i \right)_\parallel \right]}_{\Lambda_{\text{TD}}^{Y_i}} + \underbrace{\dot{\omega}_i - \dot{\omega}_c \frac{\partial Y_i}{\partial Y_{PV}}}_{\Lambda_{\text{src}}^{Y_i}}
\tag{1}
$$

$$
\rho \underbrace{\frac{\partial T}{\partial \tau}}_{\Lambda_{\text{tran}}^{T}} = \underbrace{\frac{g_c}{c_p} \frac{\partial}{\partial Y_{PV}} \left(g_c \lambda \frac{\partial T}{\partial Y_{PV}} \right) - g_c^2 \rho \sum_{i=1}^{N_s} \frac{c_{p,i}}{c_p} Y_i \widetilde{V}_i \frac{\partial T}{\partial Y_{PV}}}_{\Lambda_{\text{diff}}^{T}} + \underbrace{g_c \frac{\partial}{\partial Y_{PV}} \left(g_c \rho Y_{PV} \widetilde{V}_c \right) \frac{\partial T}{\partial Y_{PV}}}_{\Lambda_{\text{conv}}^{T}}
$$
$$
+ \underbrace{\left[-\kappa_c \left(g_c \rho \frac{\lambda}{\rho c_p} - g_c \rho Y_{PV} \widetilde{V}_c \right) \frac{\partial T}{\partial Y_{PV}} \right]}_{\Lambda_{\text{curv}}^{T}} + \underbrace{\left[-\nabla \cdot \left(\lambda \nabla_\parallel T \right) - \sum_{i=1}^{N_s} \frac{c_{p,i}}{c_p} \left(\rho Y_i \overrightarrow{V}_i \right)_\parallel \cdot \nabla T \right]}_{\Lambda_{\text{TD}}^{T}}
\tag{2}
$$
$$
+ \underbrace{\frac{\dot{\omega}_T}{c_p} - \dot{\omega}_c \frac{\partial T}{\partial Y_{PV}}}_{\Lambda_{\text{src}}^{T}}
$$

Here, ρ is the density, τ the Lagrangian-like time, Y_{PV} the reaction progress variable, g_c the magnitude of Y_{PV} gradient, i.e., $g_c = |\nabla Y_{PV}|$, $\widetilde{V}_i$ the diffusion velocity of species i in progress variable space, κ_c the flame curvature, i.e., $\kappa_c = -\nabla \cdot \overrightarrow{n} = -\nabla \cdot (\nabla Y_{PV}/|\nabla Y_{PV}|)$, $\dot{\omega}_i$ and $\dot{\omega}_c$ the reaction rate of species i and the source term of reaction progress variable, respectively, T the temperature, c_p the specific heat capacity, λ the heat conductivity, and $\dot{\omega}_T$ the heat release rate. The physical meaning of each term is indicated, including the transient term Λ_{tran}, the normal diffusion term Λ_{diff}, the convection term Λ_{conv}, the curvature term Λ_{curv} and the reaction source term Λ_{src}.

Note that Eqs. (1) and (2) also include the tangential diffusion term Λ_{TD}, which describes the diffusion along the isosurface of reaction progress variable. In 1D flamelet solutions, described in the next subsection, the tangential diffusion terms Λ_{TD} are *not* included. The tangential diffusion term Λ_{TD} is included in the above equations just to ensure the balance for the *budget* analysis,

9

where Λ_{TD} is calculated from the reference solutions,

$$\underbrace{\left(\frac{\partial \Phi \overrightarrow{V}}{\partial x_j}\right)_{\parallel}}_{\Lambda^{\Phi}_{\mathrm{TD}}} = \underbrace{\left(\frac{\partial \Phi \overrightarrow{V}}{\partial x_j}\right)}_{\Lambda^{\Phi}_{\mathrm{REF}}} - \underbrace{\left(\frac{\partial \Phi \overrightarrow{V}}{\partial x_j}\right)_{\perp}}_{\Lambda^{\Phi}_{\mathrm{norm}}} \tag{3}$$

where $\overrightarrow{V}$ represents the diffusion velocity or the gradient of temperature in physical space $\overrightarrow{x}$, and Φ stands for ρY or λ/c_p for the species mass fraction and temperature equations, respectively.

To quantify the importance of differential diffusion, the governing equation of the Bilger mixture fraction Z_{Bilger} [21] in the reaction progress variable space is newly formulated in this work and analyzed as follows,

$$\underbrace{\rho \frac{\partial Z_{\mathrm{Bilger}}}{\partial \tau}}_{\Lambda^Z_{\mathrm{tran}}} = \underbrace{\frac{1}{\beta_2 - \beta_1} \sum_{l=1}^{N_e} \gamma_l \left[\sum_{i=1}^{N_s} Z_{l,i} g_c \frac{\partial}{\partial Y_{PV}} \left(g_c \rho Y_i \widetilde{V}_i \right) \right]}_{\Lambda^Z_{\mathrm{diff}}} + \underbrace{g_c \frac{\partial}{\partial Y_{PV}} \left(g_c \rho Y_{PV} \widetilde{V}_c \right) \frac{\partial Z_{\mathrm{Bilger}}}{\partial Y_{PV}}}_{\Lambda^Z_{\mathrm{conv}}}$$

$$\underbrace{- \kappa_c \left[g_c \rho Y_{PV} \widetilde{V}_c \frac{\partial Z_{\mathrm{Bilger}}}{\partial Y_{PV}} + \frac{1}{\beta_2 - \beta_1} \sum_{l=1}^{N_e} \gamma_l \left(\sum_{i=1}^{N_s} Z_{l,i} g_c \rho Y_i \widetilde{V}_i \right) \right]}_{\Lambda^Z_{\mathrm{curv}}} + \underbrace{\left(-\dot{\omega}_c \frac{\partial Z_{\mathrm{Bilger}}}{\partial Y_{PV}} \right)}_{\Lambda^Z_{\mathrm{src}}} \tag{4}$$

$$+ \underbrace{\frac{-1}{\beta_2 - \beta_1} \sum_{l=1}^{N_e} \gamma_l \left[\sum_{i=1}^{N_s} Z_{l,i} \nabla \cdot \left(\rho Y_i \overrightarrow{V}_i \right)_{\parallel} \right]}_{\Lambda^Z_{\mathrm{TD}}}$$

where β_2 and β_1 are the sum of the elemental mass fractions in the pure fuel and pure oxidizer streams, respectively. The mass fraction of element l in species i is $Z_{l,i} = a_{l,i} W_l / W_i$, where $a_{l,i}$ is the number of atoms of element l in species i, W_l the molecular weight of element l, and W_i the molecular weight of species i. The variable γ_l is the weighting factor of element l in the definition of the Bilger mixture fraction [44]. The parameters N_e and N_s are the numbers of the elements and the species in the chemical reaction mechanism, respectively.

In this work, *budget* analyses are conducted for the governing equations of the species mass fraction, temperature, and Bilger mixture fraction, i.e., Eqs. (1), (2) and (4). *budget* analysis is used to identify the importance of different physical processes, including the transient phenomenon, the normal diffusion (i.e., the diffusion along the gradient of the reaction progress variable), the tangential diffusion (i.e., the diffusion along the isosurface of reaction progress variable), the convection, the curvature, and the reaction rate.

When the tangential diffusion term is not included, Eqs. (1), (2) and (4) are still unclosed and the governing equation for the gradient of reaction progress variable g_c must be additionally solved

10

[14],

$$0 = -g_c^2 \frac{\partial^2 g_c \rho Y_{PV} \widetilde{V}_c}{\partial Y_{PV}^2} + g_c^2 \frac{\partial \kappa_c \rho Y_{PV} \widetilde{V}_c}{\partial Y_{PV}} - \dot{\omega}_c \frac{\partial g_c}{\partial Y_{PV}} + g_c \frac{\partial \dot{\omega}_c}{\partial Y_{PV}} + \rho K_s g_c \qquad (5)$$

where K_s is the strain rate, i.e., $K_s = \nabla_t \cdot \overrightarrow{u_t} - (\overrightarrow{u} \cdot \overrightarrow{n}) \kappa_c$. The tangential component of $\overrightarrow{u}$ can be calculated as, $\overrightarrow{u_t} = \overrightarrow{u} - (\overrightarrow{u} \cdot \overrightarrow{n}) \cdot \overrightarrow{n}$. In the above equations, the strain rate K_s and curvature κ_c serve as the independent external parameters, and it has been shown that the flamelet solutions obtained from the canonical flame configurations in physical space can be reproduced by changing the parameters of K_s and κ_c [14–16].

3.2. Flamelet tabulation of differential diffusion, strain rate and curvature

In this subsection, the different flamelet tabulation methods for the differential diffusion, strain rate and curvature are described.
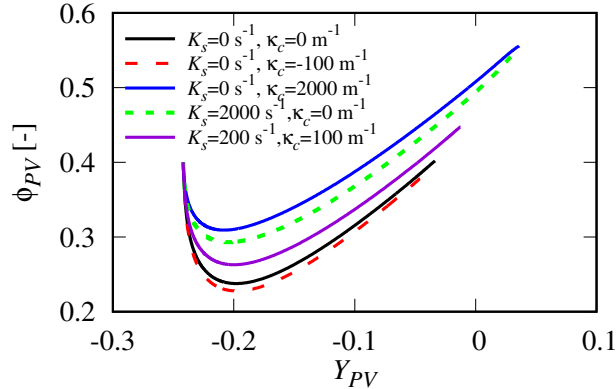

Fig. 2. Flamelet data of local equivalence ratio ϕ_{PV} in the reaction progress variable Y_{PV} ($= Y_{H_2O} - Y_{O_2} - Y_{H_2}$) space for different strain rates K_s and curvatures κ_c. The fuel mixture is H_2/air at an equivalence ratio of $\phi_0 = 0.4$ in the unburnt state and a temperature of 300 K. The diffusion flux is calculated with the mixture-averaged approach.

To incorporate the differential diffusion, strain rate and curvature, the strained-curved flamelet (SCF) equations, Eqs. (1), (2) and (5), are solved, without the transient and the tangential diffusion terms, for various values of the strain rate K_s and curvature κ_c. The diffusion flux in the strained-curved flamelet equations is calculated with the mixture-averaged approach, which is consistent with the reference simulation. The ranges of K_s and κ_c are determined from the investigated reference solutions. Differential diffusion leads to stratification within premixed flames, which can be quantified by the local mixture fraction/equivalence ratio. In Fig. 2, the local equivalence ratio ϕ_{PV} calculated for the fuel mixture of H_2/air at $\phi_0 = 0.4$ in the unburnt state and different values of K_s and κ_c is shown in the reaction progress variable Y_{PV} space. It is seen that the local

equivalence ratio changes within the reaction zone for flamelets with or without strain rate and curvature. For the H_2/air flame studied in this work, Y_{PV} is defined as, $Y_{PV} = Y_{H_2O} - Y_{O_2} - Y_{H_2}$, ensuring its bijective relationship with the thermo-chemical variables [14–16]. Note that although this definition leads to negative values of Y_{PV}, the change in Y_{PV} describes the progress of reactions. In fact, defining an optimum reaction progress variable is not straightforward, particularly for the hydrogen flame with limited number of species [45–47].

Fuel mixture stratification is observed in the reference simulation and it is caused by differential diffusion, which must be considered in the flamelet table accordingly. To this end, the premixed flamelet equations are calculated for various equivalence ratios of the unburnt H_2/air mixture ranging from 0.35 to 0.5, which fully covers the whole range of equivalence ratios in the reference simulation. The obtained flamelet solutions, referred to as Ψ, in the original flamelet look-up table can be first parameterized as a function of the boundary conditions and the solution space, i.e.,

$$\Psi = \Psi\left(\phi_{bc}, Y_{PV}, K_s, \kappa_c\right) \tag{6}$$

where ϕ_{bc} is the boundary value of the equivalence ratio for the unburnt fuel mixture. At first, ϕ_{bc} is mapped to the Bilger mixture fraction Z_{Bilger} space following the standard procedure of the flamelet-generated manifold model [19]. Same as the transport equation for Z_{Bilger}, see Eq. (4), Z_{Bilger} in the flamelet table is defined as,

$$Z_{\text{Bilger}} = \frac{\sum_{l=1}^{N_e} \gamma_l \left(\sum_{i=1}^{N_s} Z_{l,i} Y_i - \sum_{i=1}^{N_{ox}} Z_{l,i} Y_i\right)}{\sum_{l=1}^{N_e} \gamma_l \left(\sum_{i=1}^{N_{fu}} Z_{l,i} Y_i - \sum_{i=1}^{N_{ox}} Z_{l,i} Y_i\right)} \tag{7}$$

where N_{fu} and N_{ox} are the number of species in the fuel stream and oxidizer stream, respectively. For the H_2/air premixed flame studied in this work, Z_{Bilger} is calculated by setting pure H_2 as the fuel stream and pure air as the oxidizer stream. With this, the flamelet solutions are tabulated as a function of the Bilger mixture fraction Z_{Bilger}, the reaction progress variable Y_{PV}, the strain rate K_s, and the curvature κ_c,

$$\Psi = \Psi^{\text{SCF}}\left(Z_{\text{Bilger}}, Y_{PV}, K_s, \kappa_c\right) \tag{8}$$

The above tabulation method is valid under the condition that the differential diffusion can be identified by the Bilger mixture fraction. For all the trajectory variables used to tabulate the flamelet manifold, Z_{Bilger} is the only trajectory variable that characterizes the fuel stratification induced by differential diffusion. Thus, it is expected that the effects of differential diffusion can be

properly considered only if Z_{Bilger} is a suitable trajectory variable. This will be evaluated through an *a priori* analysis using the 1D flamelet solutions, in which only differential diffusion effects exist.

The strain rate K_s and curvature κ_c themselves are not the ideal trajectory variables for tabulating the thermo-chemical variables. There are two main reasons for this. On the one hand, K_s and κ_c are the instantaneous, fine-scale quantities, and the history effects of the strain rate and curvature due to convection, diffusion, reaction, etc., cannot be characterized by these two variables directly [48]. On the other hand, K_s and κ_c are a function of Y_{PV}, and a joint probability density function is required to consider the subgrid scale distributions of these trajectory variables in a large-eddy simulation; this is difficult to implement. Inspired by the previous works for tabulating the strain rate [27, 28] and curvature [12], K_s and κ_c are represented by suitable species, which characterize the flame structure's internal response to the strain rate and curvature, respectively. To this end, it is important to identify the variables that are sensitive to the strain rate and curvature.
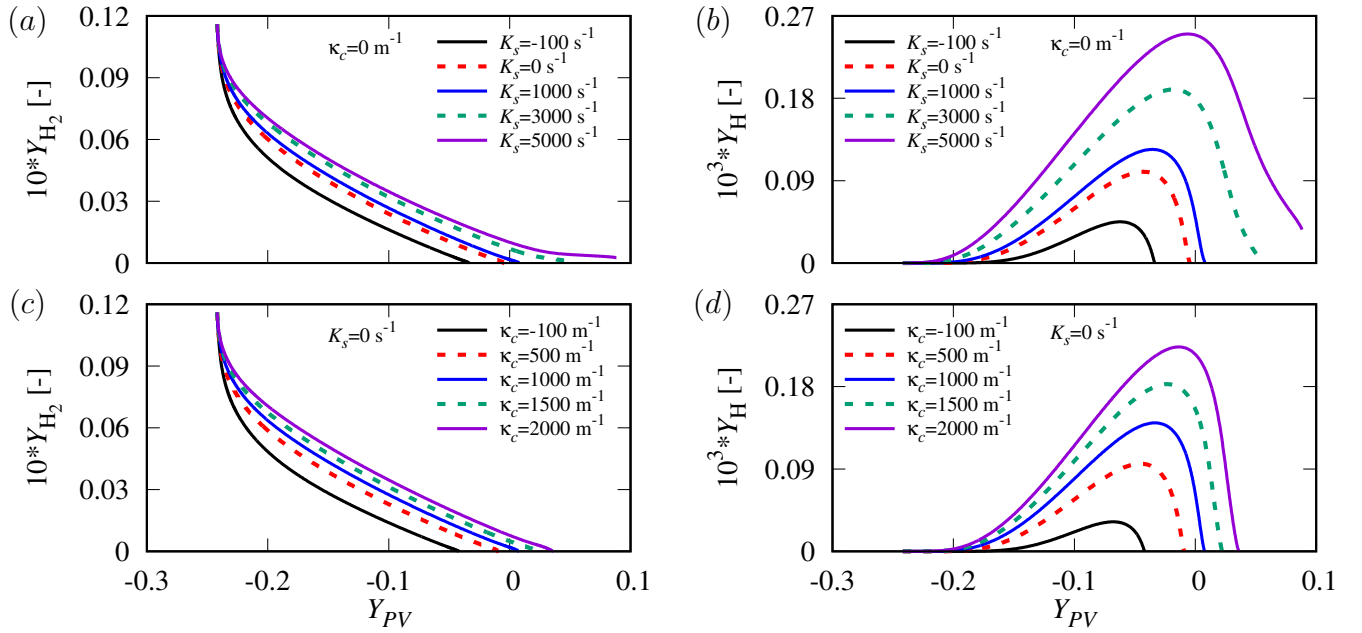

Fig. 3. Flamelet data for H_2 and H mass fractions shown in the reaction progress variable Y_{PV} space (a, b) for different strain rates K_s at a curvature of $\kappa_c = 0\,\text{m}^{-1}$, and (c, d) for different curvatures κ_c at a strain rate of $K_s = 0\,\text{s}^{-1}$. The unburnt fuel mixture is H_2/air at an equivalence ratio of 0.4, a temperature of 300 K, and a pressure of 1 atm. The diffusion flux is calculated with the mixture-averaged approach.

In Fig. 3, the flamelet data on the H_2 and H mass fractions obtained from the stationary form

of Eqs. (1), (2) and (5) are shown in the reaction progress variable Y_{PV} space for different strain rates K_s at a curvature of $\kappa_c = 0\,\mathrm{m}^{-1}$ (Figs. 3a and 3b), and for different curvatures κ_c at the strain rate of $K_s = 0\,\mathrm{s}^{-1}$ (Figs. 3c and 3d). The unburnt fuel mixture is H_2/air at an equivalence ratio of 0.4, a temperature of 300 K, and a pressure of 1 atm. The premixed flamelet equations of Eqs. (1), (2) and (5), *without* the transient and the tangential diffusion terms, are solved with the in-house code ULF [49].

As shown in Figs. 3a and 3b, the profiles of Y_{H_2} are seen to be very close to each other for a wide range of strain rates, although non-negligible differences can be seen when the strain rate becomes negative. This indicates that Y_{H_2} is not sensitive to the strain rate, particularly for positive values. Thus, Y_{H_2} is not an ideal variable to characterize the strain rate effect. By contrast, it is seen that Y_H is very sensitive to the strain rate, and the profiles of Y_H are distributed in a wide region when the strain rate is varied. The other major species are less sensitive to the strain rate (not shown for simplicity). In Figs. 3c and 3d, similar observations can be obtained as the curvature changes for a fixed value of strain rate, i.e., the profiles of Y_H vary significantly, while Y_{H_2} is rather insensitive. The behaviors of the flame structure's response to nonzero values of strain rate and curvature are provided in the Supplementary Material. It is found that with large nonzero values of strain rate and curvature, the behaviors of Y_{H_2} and Y_H are the same as those shown in Fig. 3 for $K_s = 0$ and $\kappa_c = 0$. From these observations, it can be concluded that the flame structure's response to the strain rate and curvature can be properly represented by the profile of Y_H, since it is sensitive to both strain rate and curvature. From the flamelet modeling perspective, this finding suggests that Y_H is a good candidate as trajectory variable to describe not only the sensitivity to strain rate but also the sensitivity to curvature. Finally, Fig. 3 shows that the variation range of κ_c (or K_s) is asymmetrical with a fixed value of K_s (or κ_c). This is because the flame extinguishes for significant negative values of K_s and κ_c. On the contrary, stable flames can be obtained with significant positive values of K_s and κ_c.

Based on the above findings, the flamelet solutions for the strained-curved hydrogen flame are finally tabulated as a function of the independent variables of the Bilger mixture fraction, the reaction progress variable, and the reacting variable of Y_H to represent the strain rate and curvature,

$$\Psi = \Psi^{\mathrm{MAP}}\left(Z_{\mathrm{Bilger}}, Y_{PV}, Y_H^{\mathrm{str}}, Y_H^{\mathrm{curv}}\right) \tag{9}$$

Here, the superscripts $(\cdot)^{\mathrm{str}}$ and $(\cdot)^{\mathrm{curv}}$ are introduced to differentiate the (unique) Y_H that char-

acterizes the strain rate and curvature, respectively. We note that the values for $Y_{\mathrm{H}}^{\mathrm{str}}$ and $Y_{\mathrm{H}}^{\mathrm{curv}}$ are equal, but the corresponding pair of values for strain rate and curvature can be different. This is consistent with the fact that with different combinations of the strain rate and curvature, a unique value of Y_{H} can be obtained at specific values of Z_{Bilger} and Y_{PV}. We note that this is only related to the flamelet table tabulation and flamelet table look-up. Although the values of $Y_{\mathrm{H}}^{\mathrm{str}}$ and $Y_{\mathrm{H}}^{\mathrm{curv}}$ are equal, both of them should remain in the flamelet table since they are mapped from independent trajectory variables of strain rate K_s and curvature κ_c, respectively. The suitability of this new tabulation method will be evaluated through *a priori* analyses of the reference solutions.

In summary, the mapping procedure from the original flamelet solutions as a function of the equivalence ratio of the unburnt mixture ϕ_{bc}, the progress variable Y_{PV}, the strain rate K_s, and the curvature κ_c, i.e., $\Psi\left(\phi_{bc}, Y_{PV}, K_s, \kappa_c\right)$, to the final flamelet look-up table $\Psi^{\mathrm{MAP}}\left(Z_{\mathrm{Bilger}}, Y_{PV}, Y_{\mathrm{H}}^{\mathrm{str}}, Y_{\mathrm{H}}^{\mathrm{curv}}\right)$ can be divided into three steps:

(i) The parameter ϕ_{bc} is first replaced with the Bilger mixture fraction Z_{Bilger} while the other trajectory variables of Y_{PV}, K_s and κ_c remain the same, leading to the flamelet tabulation as, $\Psi^{\mathrm{SCF}}(Z_{\mathrm{Bilger}}, Y_{PV}, K_s, \kappa_c)$, as shown in Eq. (8).

(ii) The parameter K_s is then replaced with the reacting variable $Y_{\mathrm{H}}^{\mathrm{str}}$ while the other trajectory variables of Z_{Bilger}, Y_{PV} and κ_c remain the same, leading to the flamelet tabulation as, $\Psi\left(Z_{\mathrm{Bilger}}, Y_{PV}, Y_{\mathrm{H}}^{\mathrm{str}}, \kappa_c\right)$.

(iii) Finally, κ_c is replaced with the reacting variable $Y_{\mathrm{H}}^{\mathrm{curv}}$ while the other already transformed trajectory variables of Z_{Bilger}, Y_{PV} and $Y_{\mathrm{H}}^{\mathrm{str}}$ remain the same, leading to the final flamelet look-up table as, $\Psi^{\mathrm{MAP}}\left(Z_{\mathrm{Bilger}}, Y_{PV}, Y_{\mathrm{H}}^{\mathrm{str}}, Y_{\mathrm{H}}^{\mathrm{curv}}\right)$, as shown in Eq. (9).

A similar mapping technique was also described in our previous work for partially premixed flames (see the texts before Eq. (7) in ref. [50]).

While the values of the trajectory variables of K_s and κ_c in the SCF flamelet table correspond to their boundary values for the flamelet equations, the trajectory variables of Z_{Bilger}, Y_{PV}, $Y_{\mathrm{H}}^{\mathrm{str}}$, and $Y_{\mathrm{H}}^{\mathrm{curv}}$ are discretized with 502, 251, 101 and 101 equidistant points, respectively. We find that the strongly nonlinear states induced by differential diffusion can only be identified with a sufficiently fine grid resolution for Z_{Bilger}. The prediction accuracy cannot be improved by further increasing the grid resolution.

For comparison, an additional flamelet table is generated based on the 1D freely propagating premixed (FPP) flame, without the strain rate and curvature. To take into account differential

diffusion and stratification, the flamelet solutions are obtained by solving the 1D flamelet equations for a freely propagating premixed flame in physical space for various equivalence ratios ranging from 0.35 to 3, which fully covers the whole range in the reference simulation. The diffusion flux is calculated with the mixture-averaged approach, and the temperature of the unburnt H_2/air mixture is set to 300 K, being consistent with the reference simulation. The flamelet look-up table is obtained by mapping the equivalence ratio and the physical coordinate into the Bilger mixture fraction and the reaction progress variable spaces, respectively. Finally, the obtained thermo-chemical variables are parameterized as,

$$\Psi = \Psi^{\text{FPP}} \left(Z_{\text{Bilger}}, Y_{PV} \right) \tag{10}$$

The above tabulation method is valid if the thermo-chemical variables in a premixed flame with differential diffusion can be uniquely identified by the Bilger mixture fraction and the reaction progress variable. The suitability of the above tabulation method in predicting differential diffusion has not been evaluated through an *a priori* analysis, although *a posteriori* simulations [20] and *prior* analyses [29] have been conducted. Excluding the effects of the strain rate and curvature, the suitability of using the Bilger mixture fraction to tabulate differential diffusion is evaluated on a 1D freely propagating premixed (FPP) flame through an *a priori* analysis.

4. Results and discussions

In Section 4.1, the structure of the thermodiffusively unstable flame is analyzed. Then, *budget* analyses (Section 4.2) of the premixed flamelet equations in composition space are conducted to identify the importance of the different processes in the thermodiffusively unstable flame.

4.1. Structure of the thermodiffusively unstable flame

The combustion characteristics of the thermodiffusively unstable premixed hydrogen flame have been described in detail in previous works [2, 4–8]. While the structure of the thermodiffusively unstable flame at different pressure conditions will be analyzed in Part II [51] with the linear stability theory proposed by Matalon and co-workers [3, 52], the instantaneous distributions of the OH mass fraction Y_{OH}, the Bilger mixture fraction Z_{Bilger}, the strain rate K_s and the curvature κ_c in the thermodiffusively unstable flame at atmospheric condition are shown in Fig. 4. The strain rate and curvature are calculated by conditioning on the reaction zone. This is explained
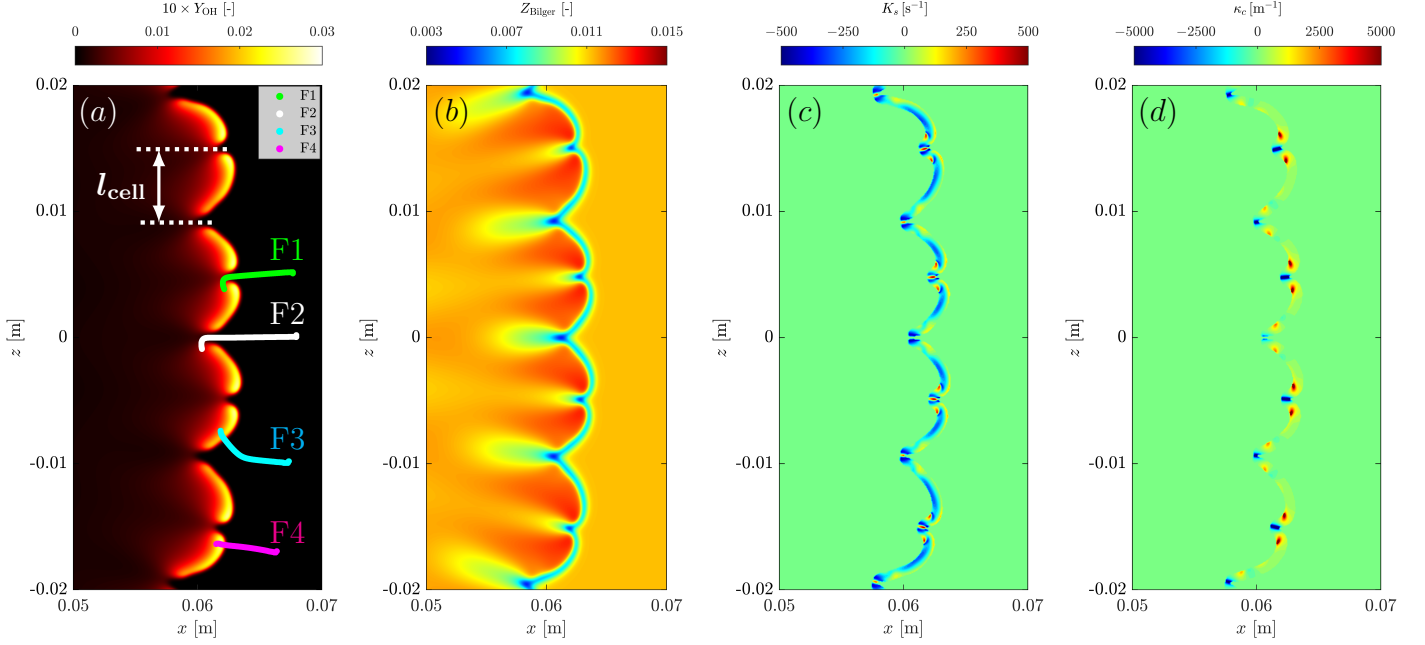
16

Fig. 4. Instantaneous distributions of (a) the OH mass fraction, (b) the Bilger mixture fraction, (c) the strain rate, and (d) the flame front curvature in the selected region indicated in Fig. 1. The representative flamelets are superimposed on the contour plot of the OH mass fraction, featuring negative curvature (F1 and F2), negligible curvature (F3) and positive curvature (F4). The strain rate and curvature are calculated by conditioning on the reaction zone.

as follows. The curvature and strain rate are defined based on the unit vector in the normal direction of the flame front, $\kappa_c = -\nabla \cdot \vec{n} = -\nabla \cdot (\nabla Y_{PV}/|\nabla Y_{PV}|)$ and $K_s = \nabla_t \cdot \vec{u_t} - (\vec{u} \cdot \vec{n}) \kappa_c$, respectively. From the mathematical point of view, the two variables are not well-defined outside the reaction zone since the value of $|\nabla Y_{PV}|$ is close to zero. From the physical point of view, it is the most meaningful to discuss strain rate and curvature for the reaction zone. To highlight the cellular structure of the thermodiffusively unstable flame, only a certain region at around the flame front is shown, as indicated in Fig. 1. The OH mass fraction is shown in Fig. 4a. It can be seen that the flame front is corrugated, with a similar length scale of the cells (l_{cell}). Note that for the outwardly propagating thermodiffusively unstable premixed hydrogen flame at atmospheric condition, wide cell length scales with finger-like flame structure, similar to that in the planar flame studied by Berger et al. [8], can be observed at later time instants with larger flame radii. As indicated by the curvature distribution, see Fig. 4d, the OH mass fraction is significant in the region with positive curvature, while it becomes small when the curvature is negative. This is due to the fact that the highly diffusive species of hydrogen tends to accumulate in the region with
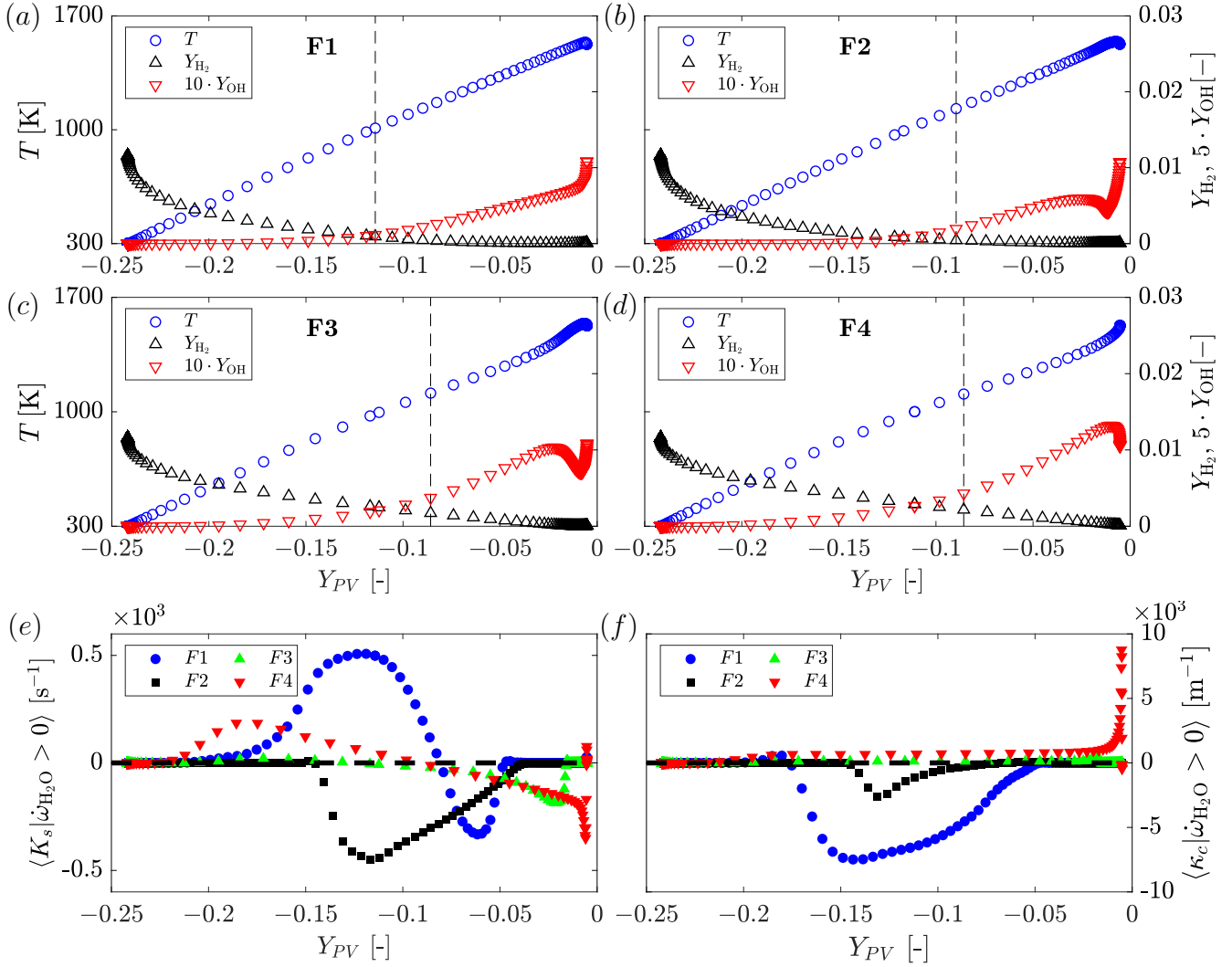
17

Fig. 5. (a-d) Thermo-chemical variables, and (e, f) the strain rate K_s and curvature κ_c for the four representative flamelets in the reaction progress variable space. The strain rate and curvature are calculated by conditioning on the reaction zone. The vertical dashed line in (a-d) indicates the location with the maximum heat release rate. The horizontal black dashed line in (e) and (f) indicates the position of zero value.

positive curvature. The distribution of the Bilger mixture fraction shown in Fig. 4b indicates that the local equivalence ratio changes significantly along the normal direction of the flame front. A richer condition is obtained in the segments with positive curvature, while the mixture is leaner in the wake region with negative curvature, see the instantaneous curvature distribution in Fig. 4d. Regarding the instantaneous distribution of the strain rate, see Fig. 4c, the strain rate value is seen to be either positive or negative at the location with positive curvature. This is associated with the fact that the strain rate depends on the balance of the velocity along the flame front and the velocity normal to the flame front, see its definition in Eq. (5), and this changes due to the local
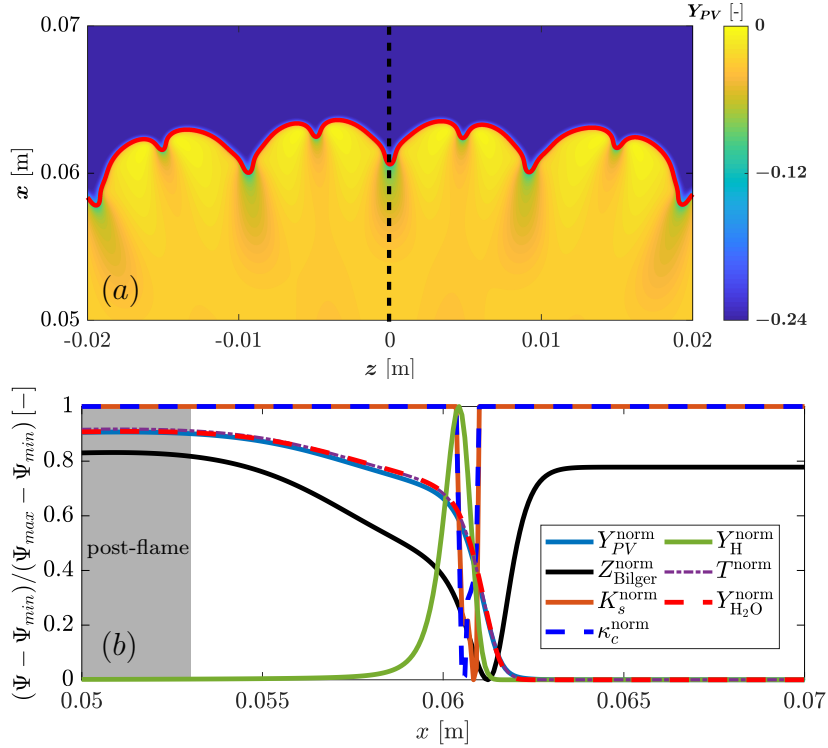
18

Fig. 6. (a) Instantaneous distribution of the progress variable in the selected region indicated in Fig. 1. The position of the iso-surface of $T_{iso} = 1000\,\mathrm{K}$ used as the starting points to extract the flamelets is indicated as the red line. (b) The instantaneous distributions of the trajectory variables used in SCF and MAP flamelet models and the thermo-chemical quantities along the vertical dashed line shown in (a). The background color in (b) indicates the post-flame zone, where the values of the trajectory variables show little change.

heat release rate. Note that there is thresholding observed in the contour plots of strain rate and curvature, which is considered due to the fact that the ranges of the color bars for these variables are much smaller than their actual limits in the reference simulation, so that the negative and positive regions can be better visualized. To challenge the capability of the proposed tabulation methods, four representative flamelets are extracted from the reference simulation, referred to as F1-F4, featuring negative curvature (F1 and F2), negligible curvature (F3), and positive curvature (F4), as indicated in Fig. 4a. The spatial location of the flamelet structure is determined according to, $d\vec{x} = (\nabla Y_{PV}/|\nabla Y_{PV}|^2)\, dY_{PV}$. The positions at the isoline of $T_{iso} = 1000\,\mathrm{K}$ are selected as the starting points, and the gradients are calculated for both directions with lower and higher temperatures. The instantaneous distribution of progress variable and the position of the isoline of $T_{iso} = 1000\,\mathrm{K}$ are shown in Fig. 6a. Note that the flamelets extracted from the reference simulation tend to turn through sharp corners on the burnt side of the flame front (see Fig. 4a), which is due to the negligible gradient of the progress variable. Actually, with a slight change

19

of the starting point on the flame front, the flamelets on the burnt side may turn to different directions. However, such a change of the flamelet direction on the burnt side does not have an effect on the evaluation of the flamelet tabulation methods, see Section 5, since the trajectory variables and the thermo-chemical states in this region do not change significantly, as shown in Fig. 6b, corresponding to the sample line in Fig. 6a. Note that the variables shown in Fig. 6b are normalized using the maximum and minimum values in the sample line.

The quantitative values of the interesting thermo-chemical variables for the four representative flamelets are shown in the reaction progress variable space, see Figs. 5a-5d. Regarding the profiles of the temperature and H_2 mass fraction, there is no obvious difference among the four representative flamelets, while the OH mass fraction shows different variation trends near the burnt sides. The quantitative values of the strain rate and curvature conditioned on the reaction zone are calculated for the representative flamelets, as shown in Figs. 5e and 5f. It is seen that F1 features strong positive and minor negative strain rates in a certain region of Y_{PV}. In the same range of Y_{PV}, a negative curvature is found in F1. In the case of F2, while it still features a negative curvature, its magnitude becomes much smaller. Unlike F1, there is only a negative strain rate in F2. For F3 extracted at the waist region of the cell, both strain rate and curvature are negligible. For F4, significant positive curvature can be seen near the burnt side, while both positive and negative strain rates exist throughout the reaction zone. The features of the four representative flamelets extracted from the reference simulation are summarized in Table 1.

Table 1. Features of the four representative flamelets extracted from the reference simulation.

Flamelets	F1	F2	F3	F4
Strain rate	$\pm$	$-$	$-$ (small)	$\pm$
Curvature	$-$	$-$	≈ 0	$+$

4.2. Budget analysis of the strained-curved flamelet equations

To understand the underlying physics of the four representative flamelets, *budget* analyses are conducted for the governing equations of the H_2 species mass fraction, temperature and Bilger mixture fraction, see Eqs. (1), (2) and (4). In Fig. 7, the budget terms of the H_2 mass fraction Y_{H_2} flamelet equation are compared in the reaction progress variable space. The balance term is calculated by subtracting the other terms from the transient term. It is clearly seen that for
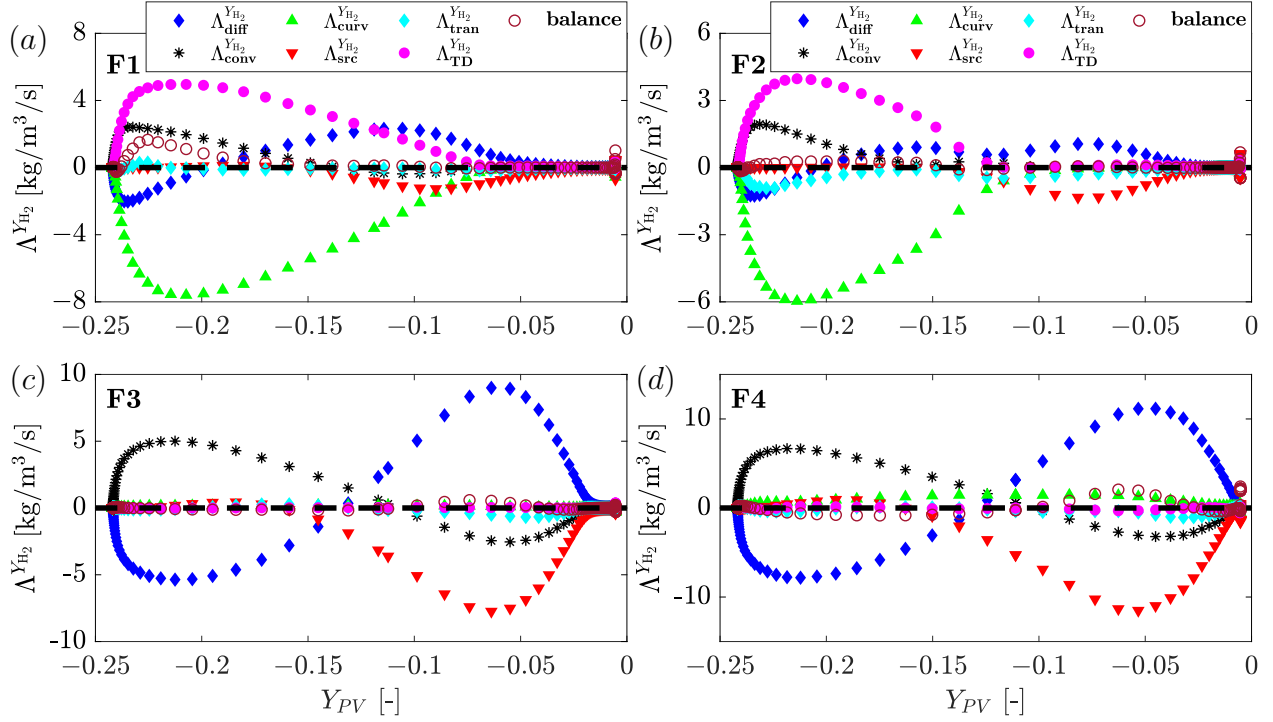
Fig. 7. Comparing the budget terms of H_2 mass fraction Y_{H_2} flamelet equation in the reaction progress variable space, see Eq. (1). The balance term is calculated by subtracting the other terms from the transient term. The horizontal black dashed line indicates the position of zero value.

F1 and F2, the curvature term $\Lambda_{\mathrm{curv}}^{Y_{H_2}}$ is significant, and balances with the tangential term $\Lambda_{\mathrm{TD}}^{Y_{H_2}}$. This indicates that at the location with negative curvature, the diffusion along the curved flame front (i.e., the tangential diffusion) is dominant, which will be explained in the following context. Note that the tangential diffusion term Λ_{TD} is not included in the 1D flamelet equations when generating the strained-curved flamelet table, which challenges the suitability of the proposed flamelet tabulation method, particularly for F1 and F2. The performance of the flamelet tabulation method in predicting the flamelets with negative curvature will be evaluated in the next subsection.

For F3, it is seen that both the curvature term $\Lambda_{\mathrm{curv}}^{Y_{H_2}}$ and the tangential diffusion term $\Lambda_{\mathrm{TD}}^{Y_{H_2}}$ are negligible, compared to the other budget terms. The diffusion normal to the flame front $\Lambda_{\mathrm{diff}}^{Y_{H_2}}$ is significant, and balances with the convection term $\Lambda_{\mathrm{conv}}^{Y_{H_2}}$ and the reaction source term $\Lambda_{\mathrm{src}}^{Y_{H_2}}$. This indicates that the flamelet solutions obtained from the 1D flamelet equations without the tangential term are expected to be valid for F3. For F4, it is seen that the curvature term $\Lambda_{\mathrm{curv}}^{Y_{H_2}}$ is negligible compared to the normal diffusion term $\Lambda_{\mathrm{diff}}^{Y_{H_2}}$ and the reaction source term $\Lambda_{\mathrm{src}}^{Y_{H_2}}$. It is important to point out that unlike the flamelets with negative curvature, the tangential diffusion

21

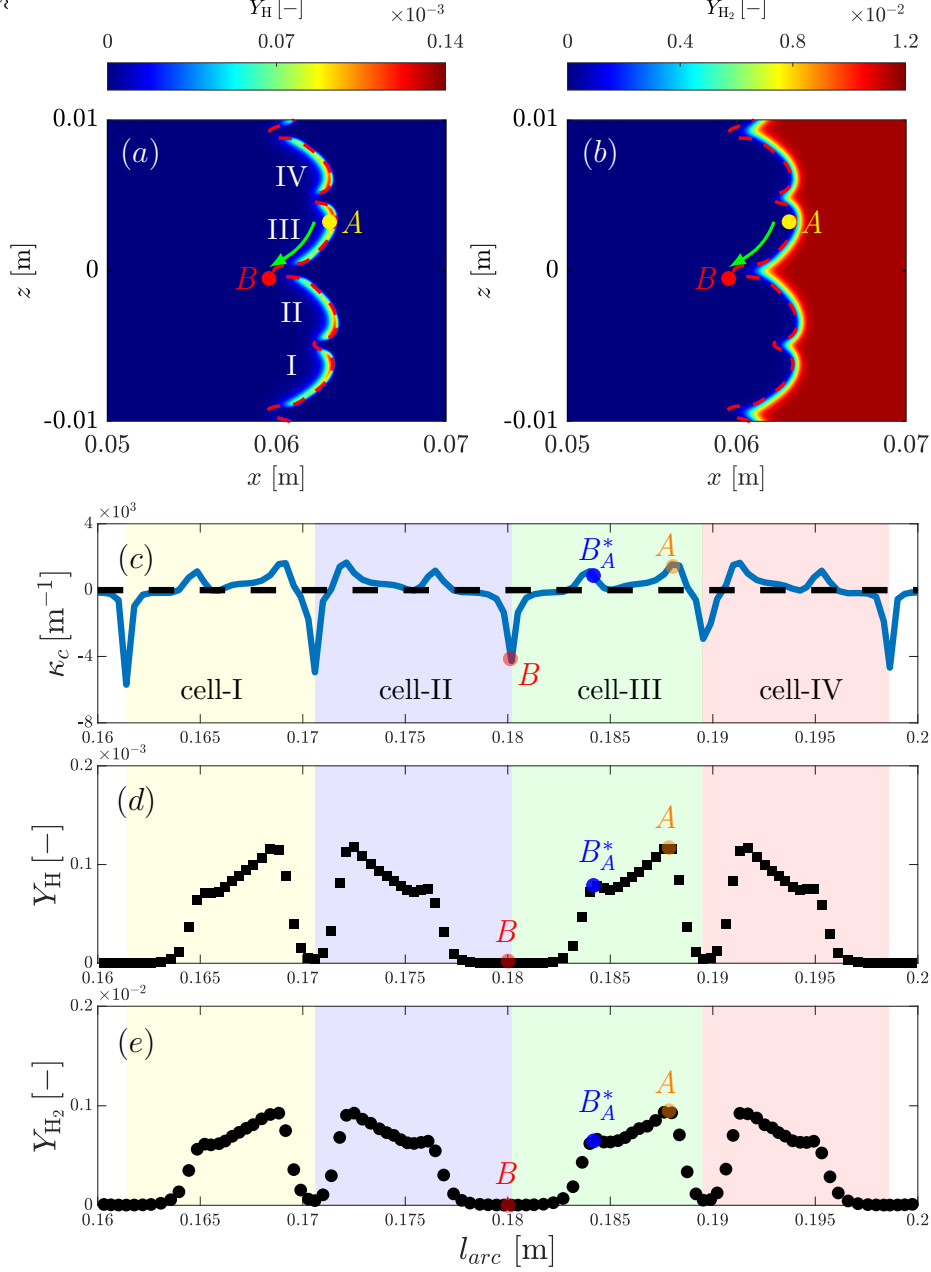term $\Lambda_{\text{TD}}^{Y_{\text{H}_2}}$ is negligible in the flamelets with positive curvature.

Fig. 8. (a, b) Contour plots of Y_{H} and Y_{H_2} in a selected region to show the representative cell structure. A representative position in the reaction zone is indicated by the red dashed line, i.e., $Y_{PV} = -0.08$. Point A is located in the positive curvature region, while point B is in the negative region. (c-e) κ_c, Y_{H} and Y_{H_2} along the flame front. The location of the flame front is defined as the arc length, $l_{arc}^{(n+1)} = l_{arc}^{(n)} + \sqrt{(dx)^2 + (dz)^2}$, with n being the point index along the Y_{PV}-isoline. The starting point, i.e., $n = 0$, is at the minimum values of x and z. The background color in (c-e) indicates the different cells in the selected region shown in (a) and (b). The positions of point A and point B in cell-III are indicated in (c)-(e). Point B_A^* indicates the local peak between A and B. The horizontal black dashed line in (c) indicates the position of zero value.

To explain the reason for the different tangential diffusion behaviors in the flame front with
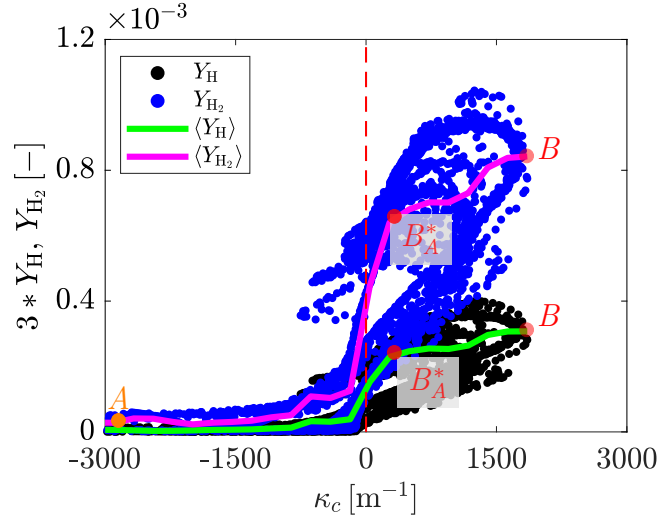
Fig. 9. Instantaneous scatter data and conditional values (solid lines) of Y_H and Y_{H_2} extracted along the isoline of $Y_{PV} = -0.08$ for the whole flame front. The vertical dashed line indicates the location of $\kappa_c = 0$. Point A and point B indicate the peaks in the negative and positive regions, respectively. Point B_A^* indicates the local peaks between A and B.

negative and positive curvatures, a representative cellular flame front is selected, as shown in Fig. 8. The contour plots of the mass fractions of H and H_2 in the investigated region are shown in Figs. 8a and 8b. A representative position in the reaction zone is indicated by the red dashed line, which corresponds to the isoline of the progress variable of $Y_{PV} = -0.08$. This value of Y_{PV} is selected since its isoline crosses the location of peak Y_H in the selected region. Point A is selected at the location with positive curvature, while point B corresponds to the location with negative curvature in the same cell. The number of cells in the selected region are indicated as I $\sim$ IV in Fig. 8a. The distributions of κ_c, Y_H and Y_{H_2} along the isoline of $Y_{PV} = -0.08$ are shown Figs. 8c-8e. The location of the flame front is characterized with the arc length, which is defined as $l_{arc}^{(n+1)} = l_{arc}^{(n)} + \sqrt{(\mathrm{d}x)^2 + (\mathrm{d}z)^2}$, with n being the point index along the Y_{PV}-isoline. The starting point to calculate the arc length, i.e., $n = 1$, is at the minimum values of x and z. The background color in Figs. 8c-8e indicates the different cells in the selected region shown in Figs. 8a and 8b, while the positions of point A and point B in cell-III are also indicated. It can be seen that, compared to point B, which has negative curvature, Y_H and Y_{H_2} are larger at point A, which has positive curvature, since the highly diffusive species of H and H_2 tend to accumulate in the positively curved region with small flame surface, while in the negatively curved region, these species have to "fill in" the larger pit, which leads to a fuel-leaner mixture. Thus, tangential

diffusion is generated between point A and point B. We note that a local peak exists between point A and point B for both Y_H and Y_{H_2}, as indicated by point B_A^*, which corresponds to a local peak of positive κ_c. This phenomenon can also be found at the other cells. The existence of the second stage of Y_H and Y_{H_2} makes the gradient between point B_C^* and point B be more significant than that between point A and point B_C^*, which explains the larger tangential diffusion term in F1 and F2 than in F4, see Fig. 7. In fact, at the positively curved flame front the concentrations of H and H_2 remain almost unchanged. In contrast, at negatively curved location, local extinction can be observed. Note that tangential diffusion will not be generated at point B with zero gradients of Y_H and Y_{H_2}, but between point B and the neighboring peak at B_A^*. Without tangential diffusion, the 1D flamelet solutions already show that negative curvature has more significant effects on Y_H and Y_{H_2} than positive curvature, as shown in Fig. 3.

To demonstrate the generality of the above finding, the instantaneous scatter data and conditional data of Y_H and Y_{H_2} extracted from the isoline of Y_{PV} are plotted in the curvature space, as shown in Fig. 9. It is found that the amounts of Y_H and Y_{H_2} in the positively curved flame front are much larger than those in the negatively curved flame front, which suggests the existence of tangential diffusion. From the conditioned data of Y_H and Y_{H_2}, a second stage can be observed between the negative curvature and the peak of the positive curvature, as indicated by point B_A^*, which is similar to the observations from the instantaneous data at cells shown in Fig. 8.

From the above observations, it can be concluded that the tangential diffusion is important for flamelets with negative curvature, while it is negligible for flamelets with positive curvature. Thus, it is important to investigate the extent to which the flamelets with negative curvatures (F1 and F2) can be reproduced using the proposed flamelet tabulation methods, in which the tangential diffusion is not included in the flamelet tables. This will be presented in the next subsection.

Figure 10 shows the budget terms of the gas temperature flamelet equation in the reaction progress variable space, see Eq. (2). For F1 and F2, it can be seen that the curvature term Λ_{curv}^T and the tangential diffusion term Λ_{TD}^T are not significant compared to the other budget terms, which is different from the results obtained for the Y_{H_2} flamelet equation, shown in Fig. 7. This indicates that the negative curvature does not generate any significant diffusion of temperature along the flame front. For F3, it is seen that only the normal diffusion term Λ_{diff}^T, the convection term Λ_{conv}^T and the reaction source term Λ_{src}^T are significant, and balance each other. The curvature term Λ_{curv}^T and the tangential diffusion term Λ_{TD}^T are negligible, as expected. For F4, the curvature
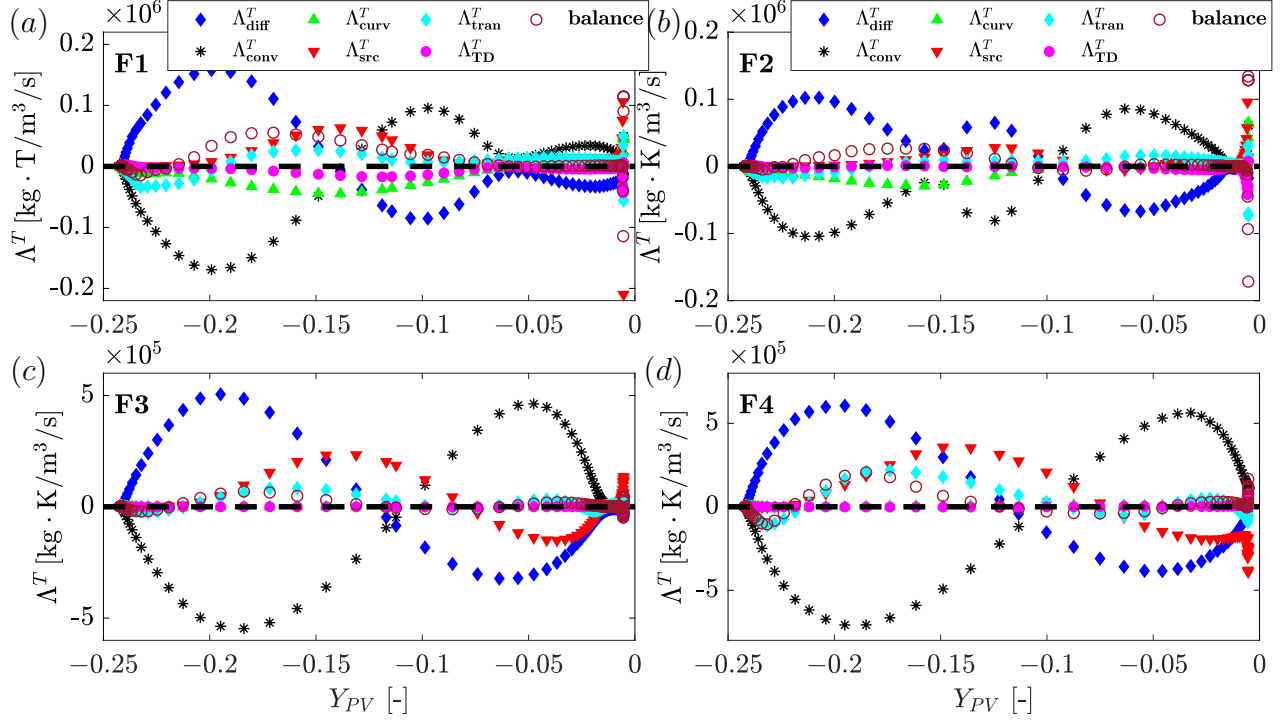
Fig. 10. Comparing the budget terms of the gas temperature T flamelet equation in the reaction progress variable space, see Eq. (2). The balance term is calculated by subtracting the other terms from the transient term. The horizontal black dashed line indicates the position of zero value.

term Λ_{curv}^T and the tangential diffusion term Λ_{TD}^T are seen to be negligible compared to the other budget terms, which indicates that the positive curvature also does not generate any significant tangential diffusion. From these observations, the curvature is not expected to have any obvious effects on the performance of the flamelet model in predicting the temperature.

Finally, the budget terms of the Bilger mixture fraction flamelet equation, see Eq. (4), are compared in Fig. 11. For F1 and F2, the curvature term Λ_{curv}^Z is seen to be of the same order of magnitude as the normal diffusion term Λ_{diff}^Z, which indicates that the negative curvature has significant effects on the local distribution of the species mass fractions. Interestingly, the tangential diffusion term Λ_{TD}^Z is seen to be one order of magnitude lower than the curvature term Λ_{curv}^Z, which indicates that the overall tangential diffusion effect is not significant for the hydrogen flame studied. This is explained by the fact that the tangential diffusion is in opposite directions for the lower Lewis number species such as H and H_2 and the larger Lewis number species such as O_2 and H_2O, which compensates for the overall tangential diffusion for the scalar Z_{Bilger}. For F3, only the normal diffusion term Λ_{diff}^Z and the convection term Λ_{conv}^Z are significant, and balance each
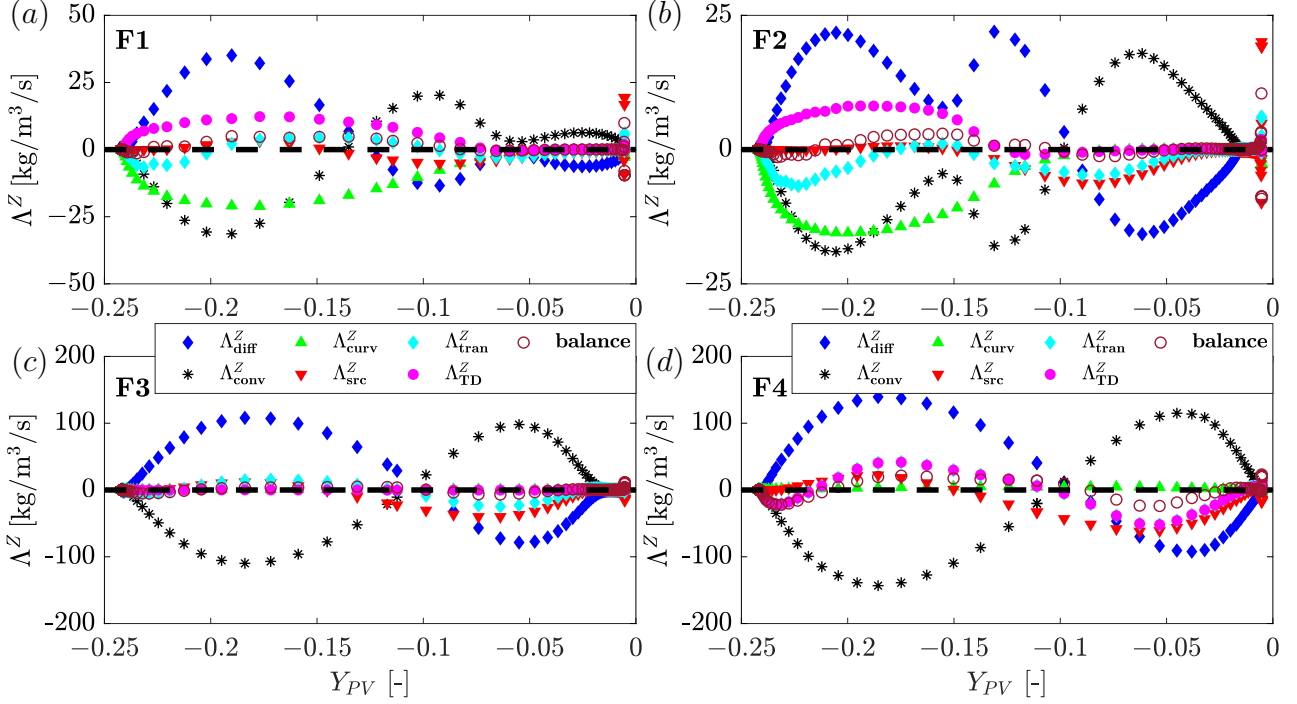
Fig. 11. Comparison between the budget terms of Bilger mixture fraction Z_{Bilger} flamelet equation in the reaction progress variable space, see Eq. (4). The balance term is calculated by subtracting the other terms from the transient term. The horizontal black dashed line indicates the position of zero value.

other. The curvature term Λ^Z_{curv} and the tangential diffusion term Λ^Z_{TD} are negligible, as expected. For F4, the normal diffusion term Λ^Z_{diff} and the convection term Λ^Z_{conv} are still dominant, and are one order of magnitude larger than the other budget terms. From these observations, it can be concluded that the negative curvature affects the overall species distribution and may influence the performance of the flamelet models, while the positive curvature does not affect the overall species distribution significantly.

5. Verification of flamelet tabulation methods

In this section, the suitability of the flamelet tabulation methods, i.e., $\Psi^{\text{SCF}}(Z_{\text{Bilger}}, Y_{PV}, K_s, \kappa_c)$ and $\Psi^{\text{MAP}}(Z_{\text{Bilger}}, Y_{PV}, Y_H^{\text{str}}, Y_H^{\text{curv}})$, in predicting differential diffusion, the strain rate and curvature is verified through an *a priori* analysis. For the *a priori* analysis, the representative flamelets described in the last section, i.e., F1-F4, are taken as the reference results. Specifically, the trajectory variables in the SCF and MAP flamelet tables are calculated from the reference representative flamelets. Then, the values extracted from the different flamelet tables are compared to the corresponding results in the representative flamelets.

Before verification of the trajectory variables in characterizing the strain rate and curvature in Section 5.2, i.e., K_s and κ_c in the SCF flamelet tabulation method, and Y_H^{str} and Y_H^{curv} in the MAP flamelet tabulation method, the suitability of the remaining trajectory variables of Z_{Bilger} and Y_{PV} is evaluated in Section 5.1.
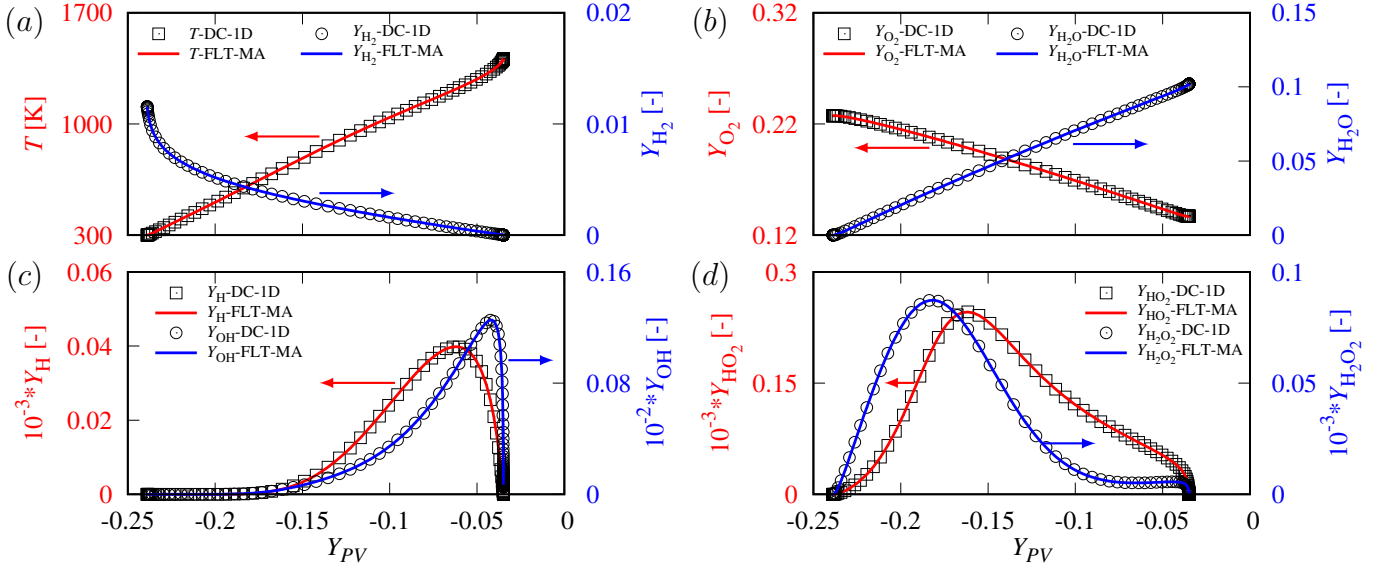
5.1. Flamelet model for differential diffusion

Fig. 12. Profiles of various thermo-chemical variables for the 1D freely propagating premixed flame at $\phi_0 = 0.4$, $T_0 = 300\,\text{K}$ and $p = 1\,\text{atm}$, comparing the detailed chemistry (DC) solutions (scatter points) and the *a priori* flamelet predictions (solid lines). The evaluated flamelet look-up table (FLT) is, $\Psi^{\text{FPP}}(Z_{\text{Bilger}}, Y_{PV})$, calculated based on the 1D freely propagating premixed flame in physical space for various equivalence ratios using the mixture-averaged approach.

At first, the suitability of the trajectory variable Z_{Bilger} in characterizing the differential diffusion is evaluated. To exclude transient and tangential diffusion effects, the flamelet model is first evaluated on a 1D freely propagating premixed (FPP) flame at $\phi_0 = 0.4$, $T_0 = 300\,\text{K}$ and $p = 1\,\text{atm}$. The detailed chemistry (DC) solutions are obtained by solving the 1D flamelet equations in physical space for all the species mass fractions and temperature based on the mixture-averaged (MA) approach. The flamelet lookup table (FLT) is calculated with the same mass diffusion model based on the 1D freely propagating premixed flame. The thermo-chemical variables are tabulated as, $\Psi^{\text{FPP}}(Z_{\text{Bilger}}, Y_{PV})$. The flamelet predictions, referred to as "FLT-MA", are compared to the corresponding DC solutions, referred to as "DC-1D", in Fig. 12. It can be seen that the thermo-chemical quantities extracted from the FLT agree very well with the reference DC solutions,
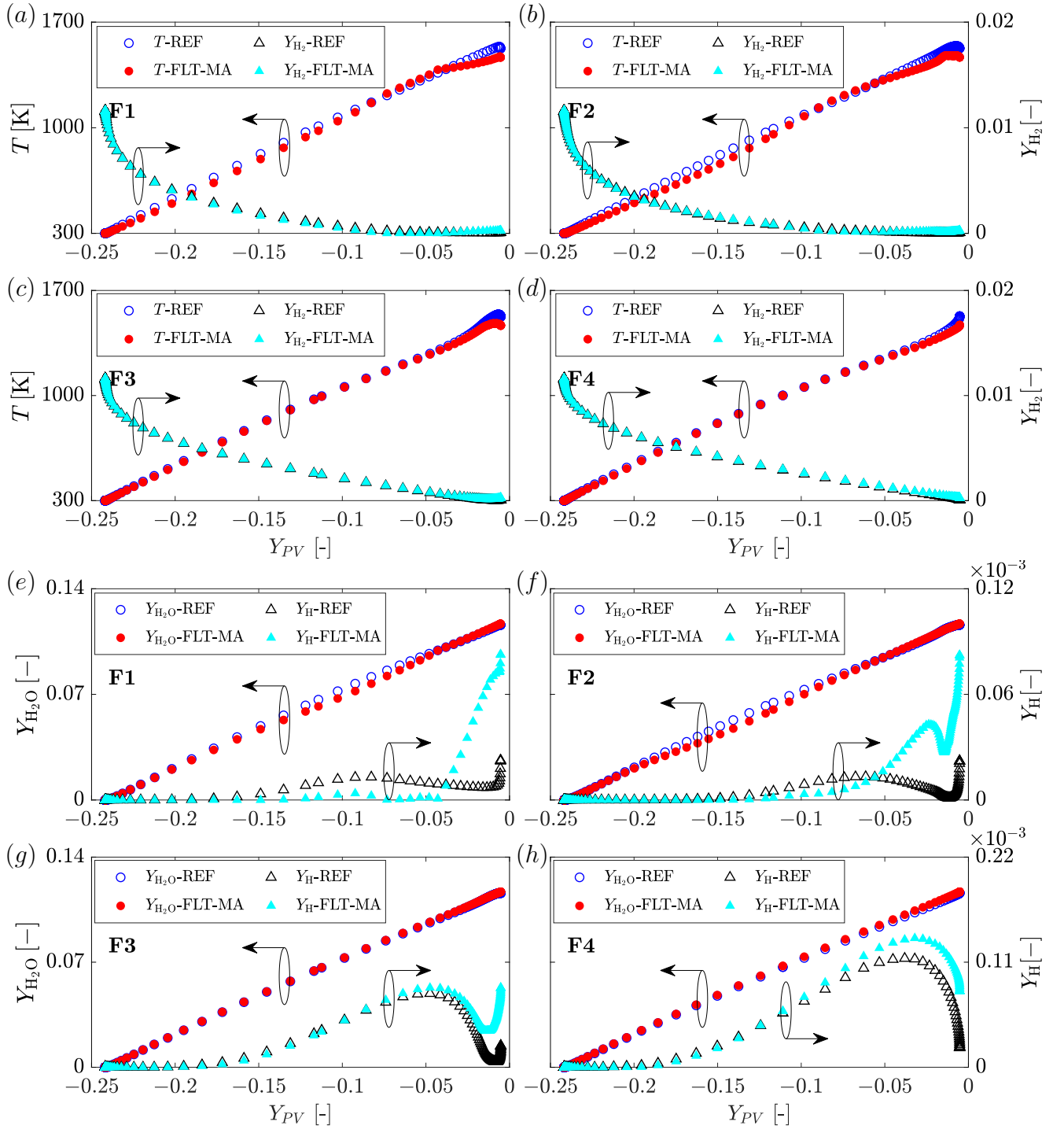
27

Fig. 13. Profiles of (a-d) temperature and H_2 mass fraction, and (e-h) H_2O and H mass fractions, comparing the reference flamelets F1-F4 extracted from the reference simulation results and the *a priori* flamelet predictions. The evaluated flamelet look-up table (FLT) is, $\Psi^{FPP}\left(Z_{Bilger}, Y_{PV}\right)$, calculated based on the 1D freely propagating premixed flame in physical space using the mixture-averaged approach.

including both the major species and the species of H and H_2. We find that the tabulated values obtained from the FLT calculated with the unity Lewis number show large discrepancies compared

with the reference results (not shown for clarity), especially for the minor species of H, OH, etc. This finding confirms that the pure differential diffusion effects can be accurately considered by the tabulation method of $\Psi^{\mathrm{FPP}}\left(Z_{\mathrm{Bilger}}, Y_{PV}\right)$, if differential diffusion is incorporated in the flamelet table.

After the suitability of the FLT is confirmed in predicting differential diffusion in the 1D configuration, the same flamelet table and the tabulation method of $\Psi^{\mathrm{FPP}}\left(Z_{\mathrm{Bilger}}, Y_{PV}\right)$ are evaluated in the four representative flamelets extracted from the reference simulation. In Fig. 13, the flamelet predictions are compared to the reference reference solutions, referred to as "REF". For the gas temperature and H_2 mass fractions, as shown in Figs. 13a-13d, good agreement is obtained when differential diffusion is considered in the flamelet table. For the H_2O and H mass fractions, as shown in Figs. 13e-13h, significant discrepancies can be seen for Y_{H}, particularly for F1 and F2 with negative curvature, although $Y_{\mathrm{H_2O}}$ is well predicted. The remaining discrepancies are partially due to the strain rate and curvature effects, as explained in the next subsection.
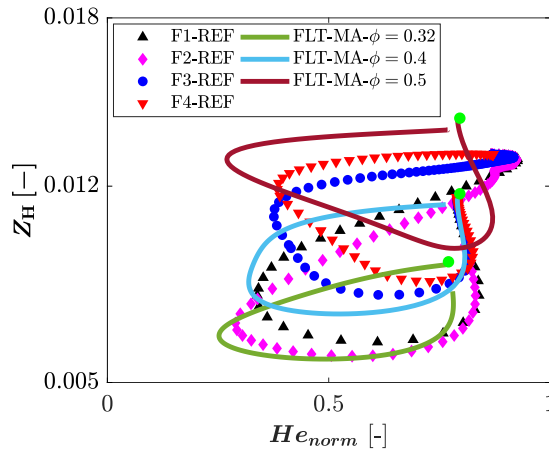

Fig. 14. Four representative flamelets (scatter points) and the 1D freely propagating premixed flamelet solutions (solid lines) obtained with the mixture-averaged approach for different equivalence ratios shown in the elemental hydrogen mixture fraction Z_{H} and the normalized total enthalpy He_{norm} space. The green filled circles indicate the unburnt states for each flamelet, which corresponds to the flamelets calculated with the unity Lewis number assumption at the same equivalence ratio.

We note that unlike the 1D configuration where only pure differential diffusion exists, F1-F4 extracted from the reference simulation have additional effects of strain rate, curvature and tangential diffusion. However, these additional phenomena are strongly coupled with differential diffusion. For example, in the thermodiffusively unstable flame studied, the strain rate, curvature

and tangential diffusion are mainly induced by the highly diffusive species of H_2. Thus, if differential diffusion is predicted, the effects induced by the strain rate and curvature were also (partially) reproduced. In other words, the agreements shown in Fig. 13 could also be due to the fact that the strain rate and curvature are partially considered by the flamelet model with differential diffusion. To validate this, we investigate whether the trajectories of the strained-curved flame in the reference simulation can be followed by the 1D freely propagating premixed flame with only differential diffusion. As shown in Fig. 14, the four representative strained-curved flamelets are shown in the elemental hydrogen mixture fraction Z_H and the normalized total enthalpy He_{norm} space. Here, Z_H represents the mass diffusivity, while He_{norm} describes the thermal diffusivity, which is defined as

$$He_{norm} = \frac{He - He_{min}^{\text{REF}}}{He_{max}^{\text{REF}} - He_{min}^{\text{REF}}} \tag{11}$$

where He_{max}^{REF} and He_{min}^{REF} are the maximum and minimum values of He in the reference simulation, respectively. For comparison, the 1D freely propagating premixed flames obtained with the mixture-averaged approach and the unity Lewis number assumption for different equivalence ratios are presented. It is clearly seen that the trajectories of the strained-curved flame in the Z_H and He_{norm} space can be roughly followed by the 1D freely propagating premixed (FPP) flames with differential diffusion, but *without* strain rate and curvature being included. In contrast, for flamelets calculated with the unity Lewis number assumption, as indicated by the green filled points in Fig. 14, they do not have trajectories in the Z_H and He_{norm} space. This indicates that the trajectories of the strained-curved flame cannot be followed by the 1D FPP flames with the unity Lewis number assumption. From the above observations, it can be concluded that differential diffusion is important in the thermodiffusively unstable flame, and the trajectories of the strained-curved flame in the reference simulation can be roughly followed by the 1D freely propagating premixed flame with only differential diffusion being considered.

After confirming the suitability of Z_{Bilger} to characterize differential diffusion, we study whether the flamelet model can predict the post-flame zone. Note that the post-flame zone, which is closely related to the NO_x emissions, is not fully covered in the representing flamelets due to the negligible gradient of Y_{PV}, see Fig. 6b. In fact, in the post-flame zone, the values of strain rate, curvature and Y_H are essentially zero (see Fig. 6b), so the thermo-chemical states are only determined by the trajectory variables of Z_{Bilger} and Y_{PV}. To evaluate the performance of the flamelet model in this region, further comparisons are conducted between the FLT and the reference simulation crossing
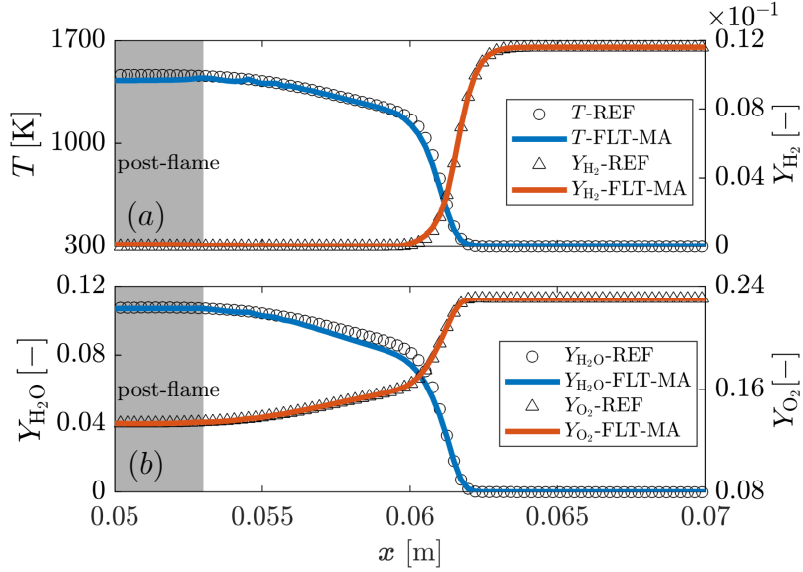
Fig. 15. Comparisons of the (a) temperature and H_2 mass fraction, and (b) H_2O and O_2 mass fractions between the reference simulation (scatter points) and the *a priori* flamelet predictions (solid lines). The flamelet look-up table $\Psi^{\mathrm{FPP}}\left(Z_{\mathrm{Bilger}}, Y_{PV}\right)$ is evaluated, which is generated based on the 1D freely propagating premixed flame in physical space using the mixture-averaged approach. The instantaneous data is extracted along the vertical line indicated in Fig. 6a. The background color indicates the post-flame zone as in Fig. 6b.

the post-flame zone in the physical space, as shown in Fig. 15. The evaluation is performed along the sample line indicated as the vertical dashed line in Fig. 6a. It can be observed that in the post-flame zone, the temperature, the reactants of H_2 and O_2, and H_2O as a major reaction product can be accurately predicted.

In summary, strong differential diffusion in the thermodiffusively unstable flame can be accurately predicted using the trajectory variables of the Bilger mixture fraction and reaction progress variable, with differential diffusion being considered in the flamelet table. However, in the case of flamelets with a significant strain rate and curvature, large discrepancies remain. In the next subsection, the strain rate and curvature will be further considered in the flamelet model to investigate whether the remaining discrepancies can be reproduced.

5.2. Strained-curved flamelet model

The strained-curved flamelet model proposed in this work is first evaluated in the 1D configuration to exclude the effects of tangential diffusion in the reference simulation. The detailed chemistry (DC) solutions are obtained from the 1D strained-curved flamelet equations, see Eqs. (1), (2) and (5) under specific strain rate and curvature conditions, with the transient and tangen-
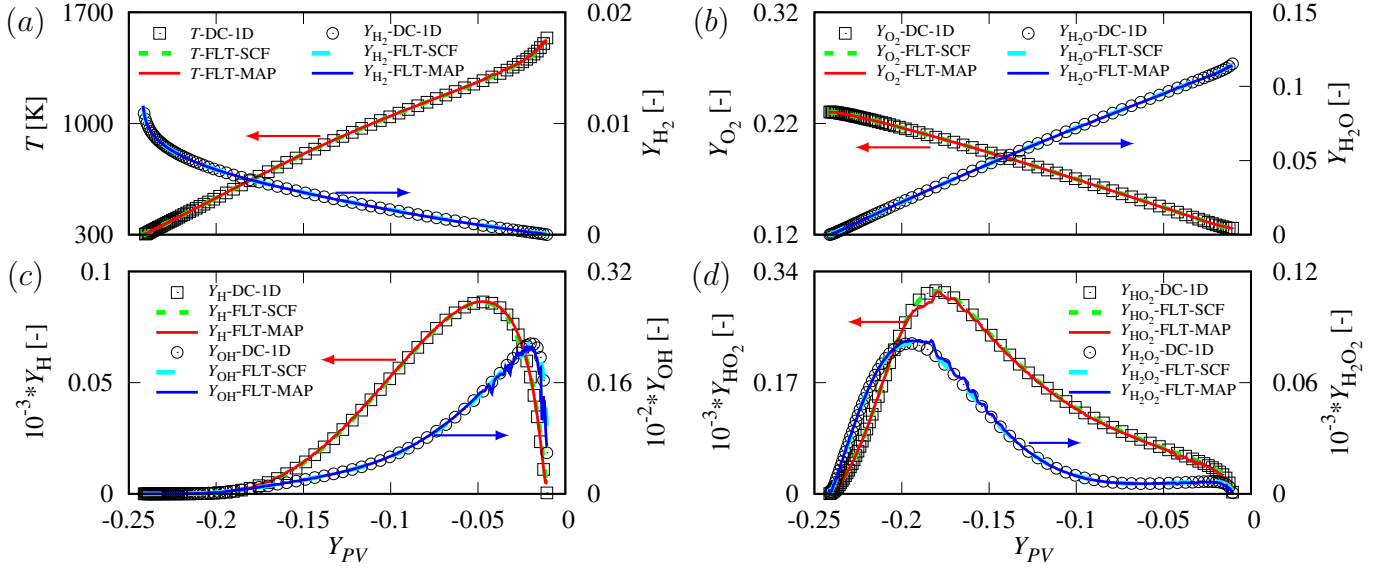
Fig. 16. Profiles of the species mass fractions for the 1D strained-curved flame, comparing the detailed chemistry (DC) solutions (scatter points) and the *a priori* flamelet predictions (dashed and solid lines). Two different flamelet look-up tables (FLT), $\Psi^{\mathrm{SCF}}\left(Z_{\mathrm{Bilger}}, Y_{PV}, K_s, \kappa_c\right)$ and $\Psi^{\mathrm{MAP}}\left(Z_{\mathrm{Bilger}}, Y_{PV}, Y_{\mathrm{H}}^{\mathrm{str}}, Y_{\mathrm{H}}^{\mathrm{curv}}\right)$, are evaluated, which are calculated based on the 1D strained-curved flamelet equations in composition space using the mixture-averaged approach. The DC solutions are obtained for a 1D strained-curved flame at $K_s = 400\,\mathrm{s}^{-1}$, $\kappa_c = -100\,\mathrm{m}^{-1}$, $\phi_0 = 0.4$ and $p = 1\,\mathrm{atm}$.

tial diffusion terms being excluded. Based on the same flamelet solutions obtained from the 1D strained-curved flamelet equations, two different tabulation methods are evaluated:

(i) The flamelet solutions are tabulated as, $\Psi^{\mathrm{SCF}}\left(Z_{\mathrm{Bilger}}, Y_{PV}, K_s, \kappa_c\right)$, using K_s and κ_c directly as the trajectory variables. This tabulation method is referred to as "SCF".

(ii) The flamelet solutions are tabulated as, $\Psi^{\mathrm{MAP}}\left(Z_{\mathrm{Bilger}}, Y_{PV}, Y_{\mathrm{H}}^{\mathrm{str}}, Y_{\mathrm{H}}^{\mathrm{curv}}\right)$, with K_s and κ_c being mapped to the reacting variable space. This tabulation strategy is referred to as "MAP".

The flamelet predictions based on the above two tabulation methods are compared to the reference detailed chemistry solutions in Fig. 16. Both flamelet tabulation methods are seen to give good predictions for both major and minor species with high diffusivity, which confirms that the flame structure's internal response to the strain rate and curvature can be described well by Y_{H}. It is noted that the profiles of Y_{OH} and $Y_{\mathrm{H}_2\mathrm{O}_2}$ are not smooth around the peak due to the numerical interpolation error in the MAP tabulation approach. We note that for a specific 1D configuration case, only single constant values of K_s and κ_c exist, which are the input values for the SCF flamelet tabulation method. However, this is not the case for Y_{H} as a trajectory variable in the
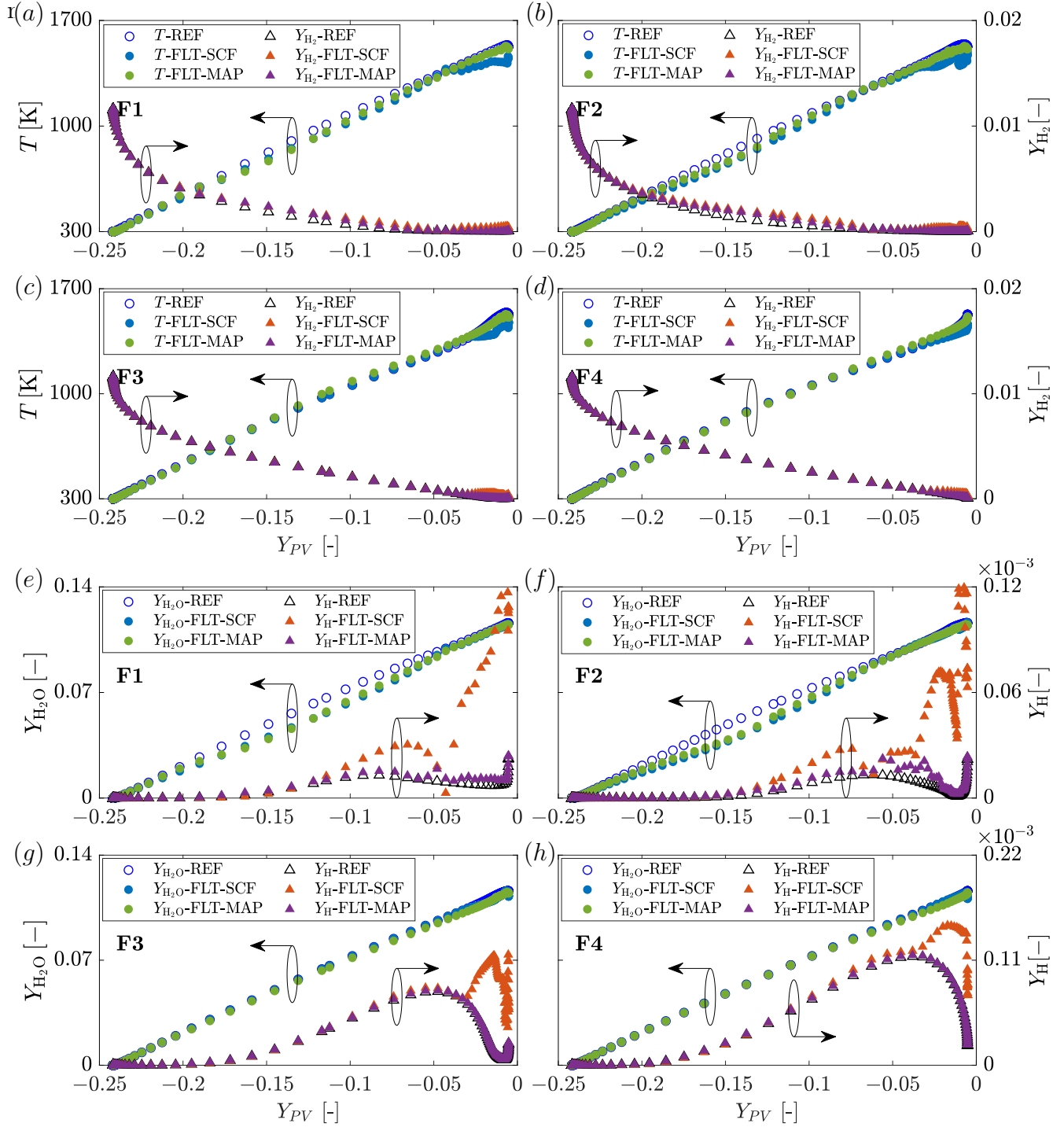
Fig. 17. Profiles of (a-d) temperature and H_2 mass fraction, and (e-h) H_2O and H mass fractions, comparing the four representative flamelets F1-F4 extracted from the reference simulation and the *a priori* flamelet predictions. Two different flamelet look-up tables (FLT), $\Psi^{\mathrm{SCF}}\left(Z_{\mathrm{Bilger}}, Y_{PV}, K_s, \kappa_c\right)$ and $\Psi^{\mathrm{MAP}}\left(Z_{\mathrm{Bilger}}, Y_{PV}, Y_{\mathrm{H}}^{\mathrm{str}}, Y_{\mathrm{H}}^{\mathrm{curv}}\right)$, are evaluated, which are calculated based on the 1D strained-curved flamelet equations in composition space using the mixture-averaged approach.

After the suitability of the flamelet tabulation methods of SCF and MAP is confirmed, they

33

are applied to the representative flamelets extracted from the reference simulation. The flamelet predictions are compared to the reference reference simulation results, as shown in Fig. 17. For the temperature and H_2 mass fraction, both the SCF and MAP flamelet models perform well in the whole Y_{PV} region. The *budget* analysis shown in Section 4.2 indicates that the processes dominating the temperature evolution are not sensitive to the strain rate and curvature, while the H_2 mass fraction evolution is affected by the strain rate and curvature. The good prediction of the H_2 mass fraction with the FLT-MA model shown in Fig. 13 is considered to be due to the fact that the flamelet solutions with differential diffusion can partially consider the effects of the strain rate and curvature, as explained in Fig. 14. For the H mass fraction, as shown in Fig. 17e-17h, the MAP flamelet model is seen to perform much better than the SCF flamelet model, although only a slight improvement is observed for the H_2O mass fraction. In certain regions, the SCF model performs even worse than the FLT-MA flamelet model (see Fig. 13), especially near the burnt sides. This is explained as follows. The strain rate and curvature are related to the normalized gradient of the reaction progress variable (i.e., $\overrightarrow{n} = \nabla Y_{PV}/|\nabla Y_{PV}|$). This is not suitable because the gradient of the reaction progress variable approaches zero in regions with a negligible change in Y_{PV}, e.g., the burnt sides. Note that Y_H^{str} and Y_H^{curv} as input values (i.e., the trajectory variables) for the new flamelet tabulation method, i.e., $\Psi = \Psi^{MAP}(Z_{Bilger}, Y_{PV}, Y_H^{str}, Y_H^{curv})$, do not necessarily agree well with the output value extracted from the flamelet table (i.e., the tabulated value) if the flamelet table is not properly generated or the trajectory variable is not properly selected, see Section 3 in the Supplementary Material. In fact, the accurate prediction of the input variable proves that both the flamelet table and the selected trajectory variable are valid.

The performance of the FPP, SCF and MAP tabulation methods in predicting the other intermediate species, such as OH and O, is also evaluated, as shown in Fig. 18. It is seen that the MAP model again performs much better than the FPP and SCF models, especially in the regions with significant strain rates and curvatures, which confirms the superiority of the MAP model. Compared to the SCF model, the better performance of the MAP model benefits from the following aspects. (i) The limitation in the definitions of K_s and κ_c in the SCF model is avoided by introducing Y_H as the trajectory variable. (ii) The history effects of the strain rate and curvature due to convection, diffusion, reaction, etc., can be considered by solving the transport equation for Y_H.

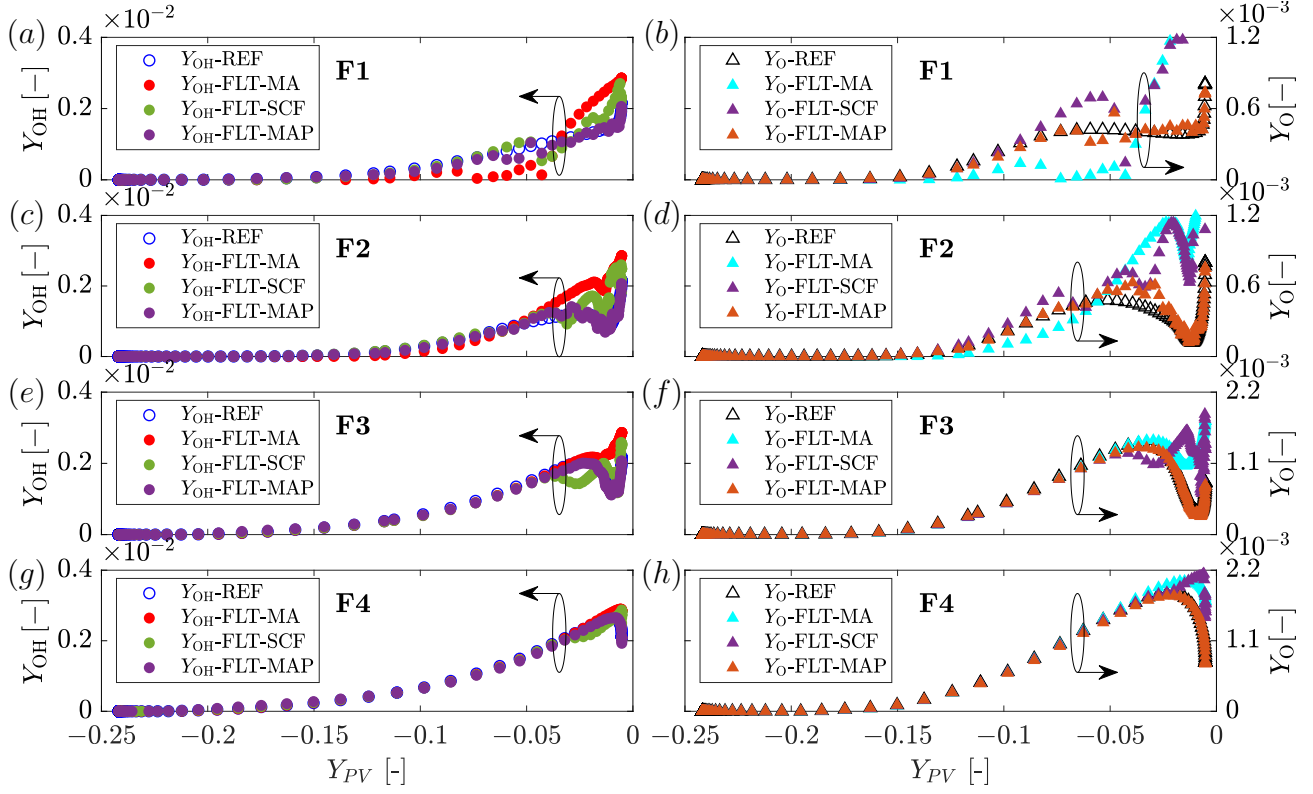The above finding confirms that the inner curved flame structure imposed by the strain rate

34

Fig. 18. Profiles of (a,c,e,g) OH mass fraction, and (b,d,f,h) O mass fraction, comparing the four representative flamelets F1-F4 extracted from the reference simulation and the flamelet predictions. Three different flamelet look-up tables (FLT), $\Psi^{\mathrm{FPP}}(Z_{\mathrm{Bilger}}, Y_{PV})$, $\Psi^{\mathrm{SCF}}(Z_{\mathrm{Bilger}}, Y_{PV}, K_s, \kappa_c)$ and $\Psi^{\mathrm{MAP}}(Z_{\mathrm{Bilger}}, Y_{PV}, Y_{\mathrm{H}}^{\mathrm{str}}, Y_{\mathrm{H}}^{\mathrm{curv}})$, are evaluated, which are calculated based on the 1D freely-propagating premixed flame, and the 1D strained-curved flamelet equations in composition space, respectively, using the mixture-averaged approach.

can be accurately predicted by the newly proposed MAP tabulation method based on the curved-strained flamelet equations. We note that tangential diffusion exists in the reference simulation, especially for highly diffusive species in F1 and F2, as evidenced by the *budget* analysis. However, the tangential diffusion term Λ_{TD} is not included when solving the strain-curved flamelet equations. Nevertheless, good agreements are achieved between the MAP flamelet predictions and the reference simulation results. The reason for this is that in the *a priori* analysis, the trajectory variables of Z_{Bilger}, Y_{PV}, $Y_{\mathrm{H}}^{\mathrm{str}}$ and $Y_{\mathrm{H}}^{\mathrm{curv}}$ are calculated from the reference simulation, in which the diffusion in all directions (including the tangential direction) is included. This is consistent with our previous findings for non-premixed flames [53].

In *a posterori* simulation, the progress variable source term $\dot{\omega}_c$, and the reaction rate of the newly introduced trajectory variable $\dot{\omega}_{\mathrm{H}}$, are extracted from the flamelet look-up table. To demonstrate the capability of the proposed flamelet tabulation method in the *a posterori* simulation, $\dot{\omega}_c$
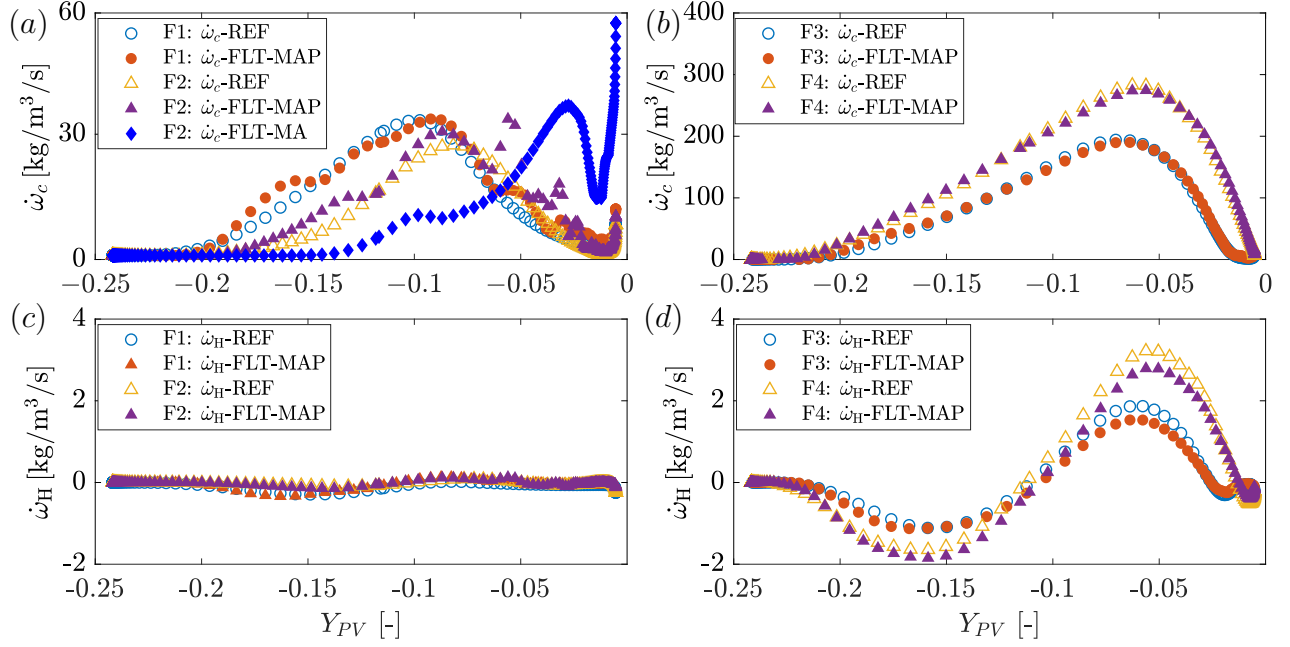
35

Fig. 19. Profiles of (a,b) the progress variable source term, $\dot{\omega}_c$, and (c,d) the reaction rate of H, $\dot{\omega}_H$, comparing the flamelets extracted from the reference simulation and the *a priori* flamelet predictions tabulated as, $\Psi^{\mathrm{MAP}}(Z_{\mathrm{Bilger}}, Y_{PV}, Y_H^{\mathrm{str}}, Y_H^{\mathrm{curv}})$. The progress variable source term $\dot{\omega}_c$ in F2 predicted with FLT-MA is also shown for comparison, which is tabulated based on the 1D freely propagating premixed flame as $\Psi^{\mathrm{FPP}}(Z_{\mathrm{Bilger}}, Y_{PV})$.

and $\dot{\omega}_H$ extracted from the flamelet table tabulated with $\Psi^{\mathrm{MAP}}(Z_{\mathrm{Bilger}}, Y_{PV}, Y_H^{\mathrm{str}}, Y_H^{\mathrm{curv}})$ are compared to the reference results extracted from the reference simulation, as shown in Fig. 19. It can be observed that for $\dot{\omega}_c$ in F1 and F2 with negative curvatures shown in Fig. 19a, the FLT-MAP tabulation method gives good predictions. In comparison, large discrepancies can be observed for $\dot{\omega}_c$ in F2 when the FLT-MA tabulation method is used, particularly near the burnt side. For F3 and F4 with negligible and positive curvatures, $\dot{\omega}_c$ is seen to be much larger than that in F1 and F2, and again good agreements are obtained. For $\dot{\omega}_H$ in F1 and F2, see Fig. 19c, its value is close to zero, which is predicted by the FLT-MAP tabulation method. For F3 and F4, the value of $\dot{\omega}_H$ becomes significant, which is again accurately predicted by FLT-MAP. The good prediction of the source terms for the trajectory variables suggests the capability of the FLT-MAP tabulation method in the *a posteriori* simulations.

In summary, the proposed mapped strained-curved flamelet model performs well in predicting the thermo-chemical variables in the thermodiffusively unstable flame. The strain rate and curvature themselves are not feasible trajectory variables.

36

6. Summary and conclusions

In this work, a multidimensional expanding, thermodiffusively unstable premixed hydrogen flame is investigated through *budget* and *a priori* analyses. The recurring issues for modeling differential diffusion, strain rate and curvature are revisited using the flamelet tabulation method. Particularly, a new flamelet tabulation method is proposed to characterize the effects of the strain rate and curvature based on the recently developed strained-curved premixed flamelet equations in composition space. The main findings obtained in this work are summarized as follows:

(i) Tangential diffusion is significant only for the highly diffusive species in the thermodiffusively unstable flame, especially for the flame front with negative curvature. The positive curvature has negligible effects on the tangential diffusion for the flame studied;

(ii) Differential diffusion can be accurately predicted by the flamelet model, with differential diffusion being considered in the flamelet table and the Bilger mixture fraction being introduced as one of the trajectory variables;

(iii) The trajectories of the strained-curved flame can be roughly followed by the 1D freely propagating premixed flames calculated at various equivalence ratios with differential diffusion being considered;

(iv) Introducing the strain rate and curvature themselves as the trajectory variables does not necessarily improve the prediction accuracy compared to the flamelet model which does not take into account the strain rate and curvature;

(v) Introducing the hydrogen mass fraction as the trajectory variable to characterize the flame structure's internal response to the strain rate and curvature can improve the prediction accuracy significantly, especially for the intermediate species mass fractions.

References

[1] M. Matalon, Intrinsic flame instabilities in premixed and nonpremixed combustion, Annu. Rev. Fluid Mech. 39 (2007) 163–191.

[2] C. K. Law, Combustion physics, Cambridge University Press, 2010.

[3] M. Matalon, C. Cui, J. Bechtold, Hydrodynamic theory of premixed flames: effects of stoichiometry, variable transport coefficients and arbitrary reaction orders, J. Fluid Mech. 487 (2003) 179.

[4] S. Kadowaki, H. Suzuki, H. Kobayashi, The unstable behavior of cellular premixed flames induced by intrinsic instability, Proc. Combust. Inst. 30 (2005) 169–176.

[5] J. Yuan, Y. Ju, C. K. Law, On flame-front instability at elevated pressures, Proc. Combust. Inst. 31 (2007) 1267–1274.

[6] M. S. Day, X. Gao, J. B. Bell, Properties of lean turbulent methane-air flames with significant hydrogen addition, Proc. Combust. Inst. 33 (2011) 1601–1608.

[7] C. Altantzis, C. Frouzakis, A. Tomboulides, M. Matalon, K. Boulouchos, Hydrodynamic and thermodiffusive instability effects on the evolution of laminar planar lean premixed hydrogen flames, J. Fluid Mech. 700 (2012) 329–361.

[8] L. Berger, K. Kleinheinz, A. Attili, H. Pitsch, Characteristic patterns of thermodiffusively unstable premixed lean hydrogen flames, Proc. Combust. Inst. 37 (2019) 1879–1886.

[9] N. Peters, Laminar diffusion flamelet models in non-premixed turbulent combustion, Prog. Energy Combust. Sci. 10 (1984) 319–339.

[10] J. van Oijen, A. Donini, R. Bastiaans, J. ten Thije Boonkkamp, L. de Goey, State-of-the-art in premixed combustion modeling using flamelet generated manifolds, Prog. Energy Combust. Sci. 57 (2016) 30–74.

[11] Y. Xuan, G. Blanquart, M. E. Mueller, Modeling curvature effects in diffusion flames using a laminar flamelet model, Combust. Flame 161 (2014) 1294–1309.

[12] M. U. Göktolga, P. de Goey, J. van Oijen, Modeling curvature effects in turbulent autoigniting non-premixed flames using tabulated chemistry, Proc. Combust. Inst. 38 (2021) 2741–2748.

[13] C. Law, C. Sung, Structure, aerodynamics, and geometry of premixed flamelets, Prog. Energy Combust. Sci. 26 (2000) 459–505.

[14] A. Scholtissek, P. Domingo, L. Vervisch, C. Hasse, A self-contained composition space solution method for strained and curved premixed flamelets, Combust. Flame 207 (2019) 342–355.

[15] A. Scholtissek, P. Domingo, L. Vervisch, C. Hasse, A self-contained progress variable space solution method for thermochemical variables and flame speed in freely-propagating premixed flamelets, Proc. Combust. Inst. 37 (2019) 1529–1536.

[16] H. Böttler, A. Scholtissek, X. Chen, Z. Chen, C. Hasse, Premixed flames for arbitrary combinations of strain and curvature, Proc. Combust. Inst. 38 (2021) 2031–2039.

[17] H. Pitsch, N. Peters, A consistent flamelet formulation for non-premixed combustion considering differential diffusion effects, Combust. Flame 114 (1998) 26–40.

[18] J. A. de Swart, R. J. Bastiaans, J. A. van Oijen, L. P. H. de Goey, R. S. Cant, Inclusion of preferential diffusion in simulations of premixed combustion of hydrogen/methane mixtures with flamelet generated manifolds, Flow Turb. Combust. 85 (2010) 473–511.

[19] J. van Oijen, L. de Goey, Modelling of premixed laminar flames using flamelet-generated manifolds, Combust. Sci. Technol. 161 (2000) 113–137.

[20] A. Donini, R. Bastiaans, J. van Oijen, L. de Goey, Differential diffusion effects inclusion with flamelet generated manifold for the modeling of stratified premixed cooled flames, Proc. Combust. Inst. 35 (2015) 831–837.

[21] R. Bilger, S. Stårner, R. Kee, On reduced mechanisms for methane/air combustion in non-premixed flames, Combust. Flame 80 (1990) 135–149.

[22] L. Verhoeven, W. Ramaekers, J. van Oijen, L. de Goey, Modeling non-premixed laminar co-flow flames using flamelet-generated manifolds, Combust. Flame 159 (2012) 230–241.

[23] L. Verhoeven, M. de Andrade Oliveira, A. Lantz, B. Li, Z. Li, C. Luijten, J. Van Oijen, M. Aldén, L. de Goey, A numerical and experimental study of Polycyclic Aromatic Hydrocarbons in a laminar diffusion flame, Proc. Combust. Inst. 34 (2013) 1819–1826.

[24] J. D. Regele, E. Knudsen, H. Pitsch, G. Blanquart, A two-equation model for non-unity Lewis number differential diffusion in lean premixed laminar flames, Combust. Flame 160 (2013) 240–250.

[25] R. Mercier, P. Auzillon, V. Moureau, N. Darabiha, O. Gicquel, D. Veynante, B. Fiorina, LES modeling of the impact of heat losses and differential diffusion on turbulent stratified flame propagation: Application to the TU Darmstadt stratified flame, Flow Turb. Combust. 93 (2014) 349–381.

[26] H. Kolla, N. Swaminathan, Strained flamelets for turbulent premixed flames, I: Formulation and planar flame results, Combust. Flame 157 (2010) 943–954.

[27] E. Knudsen, H. Kolla, E. R. Hawkes, H. Pitsch, LES of a premixed jet flame DNS using a strained flamelet model, Combust. Flame 160 (2013) 2911–2927.

[28] P. Trisjono, K. Kleinheinz, E. R. Hawkes, H. Pitsch, Modeling turbulence–chemistry interaction in lean premixed hydrogen flames with a strained flamelet model, Combust. Flame 174 (2016) 194–207.

[29] X. Wen, S. Hartl, A. Dreizler, J. Janicka, C. Hasse, Flame structure analysis of turbulent premixed/stratified flames with H_2 addition considering differential diffusion and stretch effects, Proc. Combust. Inst. 38 (2021) 2993–3001.

[30] J. van Oijen, R. Bastiaans, L. de Goey, Low-dimensional manifolds in direct numerical simulations of premixed turbulent flames, Proc. Combust. Inst. 31 (2007) 1377–1384.

[31] H. Xu, F. Hunger, M. Vascellari, C. Hasse, A consistent flamelet formulation for a reacting char particle considering curvature effects, Combust. Flame 160 (2013) 2540–2558.

[32] J. Schlup, G. Blanquart, Reproducing curvature effects due to differential diffusion in tabulated chemistry for premixed flames, Proc. Combust. Inst. 37 (2019) 2511–2518.

[33] F. Creta, P. E. Lapenna, R. Lamioni, N. Fogla, M. Matalon, Propagation of premixed flames in the presence of Darrieus–Landau and thermal diffusive instabilities, Combust. Flame 216 (2020) 256–270.

[34] Wedge boundary condition in OpenFOAM, available at https://www.openfoam.com/documentation/guides/latest/api/classFoam_1_1wedgeFvPatchField.html, 2021.

[35] F. Zhang, T. Baust, T. Zirwes, J. Denev, P. Habisreuther, N. Zarzalis, H. Bockhorn, Impact of infinite thin flame approach on the evaluation of flame speed using spherically expanding flames, Energy Technol. 5 (2017) 1055–1063.

[36] T. Zirwes, F. Zhang, J. A. Denev, P. Habisreuther, H. Bockhorn, Automated code generation for maximizing performance of detailed chemistry calculations in OpenFOAM, in: High Performance Computing in Science and Engineering'17, Springer, 2018, pp. 189–204.

[37] T. Zirwes, F. Zhang, J. A. Denev, P. Habisreuther, H. Bockhorn, D. Trimis, Improved vectorization for efficient chemistry computations in OpenFOAM for large scale combustion simulations, in: High Performance Computing in Science and Engineering'18, Springer, 2019, pp. 209–224.

[38] T. Zirwes, F. Zhang, P. Habisreuther, M. Hansinger, H. Bockhorn, M. Pfitzner, D. Trimis, Quasi-DNS dataset of a piloted flame with inhomogeneous inlet conditions, Flow Turbul.

Combust. (2019) https://doi.org/10.1007/s10494--019--00081--5.

[39] T. Zirwes, T. Häber, F. Zhang, H. Kosaka, A. Dreizler, M. Steinhausen, C. Hasse, A. Stagni, D. Trimis, R. Suntz, et al., Numerical study of quenching distances for side-wall quenching using detailed diffusion and chemistry, Flow Turbul. Combust. 104 (2020) 997–1027.

[40] H. G. Weller, G. Tabor, H. Jasak, C. Fureby, A tensorial approach to computational continuum mechanics using object-oriented techniques, Comput. Phys. 12 (1998) 620–631.

[41] D. G. Goodwin, R. L. Speth, H. K. Moffat, B. W. Weber, Cantera: An object-oriented software toolkit for chemical kinetics, thermodynamics, and transport processes, available at https://www.cantera.org, 2018. Version 2.4.0.

[42] J. Hirschfelder, R. B. Bird, C. F. Curtiss, Molecular theory of gases and liquids (1964).

[43] T. Varga, T. Nagy, C. Olm, I. G. Zsély, R. Pálvölgyi, É. Valkó, G. Vincze, M. Cserháti, H. J. Curran, T. Turányi, Optimization of a hydrogen combustion mechanism using both direct and indirect measurements, Proc. Combust. Inst. 35 (2015) 589–596.

[44] J. Sutherland, P. Smith, J. Chen, Quantification of differential diffusion in nonpremixed systems, Combust. Theor. Model. 9 (2005) 365–383.

[45] Y.-S. Niu, L. Vervisch, P. D. Tao, An optimization-based approach to detailed chemistry tabulation: Automated progress variable definition, Combust. Flame 160 (2013) 776–785.

[46] M. Ihme, L. Shunn, J. Zhang, Regularization of reaction progress variable for application to flamelet-based combustion models, J. Comput. Phys. 231 (2012) 7715–7721.

[47] U. Prüfert, S. Hartl, F. Hunger, D. Messig, M. Eiermann, C. Hasse, A constrained control approach for the automated choice of an optimal progress variable for chemistry tabulation, Flow Turbul. Combust. 94 (2015) 593–617.

[48] T. Zirwes, F. Zhang, Y. Wang, P. Habisreuther, J. A. Denev, Z. Chen, H. Bockhorn, D. Trimis, In-situ flame particle tracking based on barycentric coordinates for studying local flame dynamics in pulsating bunsen flames, Proc. Combust. Inst. 38 (2021) 2057–2066.

[49] A. Zschutschke, D. Messig, A. Scholtissek, C. Hasse, Universal Laminar Flame (ULF) solver, available at https://figshare.com/articles/ULF_code_pdf/5119855/2, 2017.

[50] X. Wen, X.-S. Bai, K. Luo, H. Wang, Y. Luo, J. Fan, A generalized flamelet tabulation method for partially premixed combustion, Combust. Flame 198 (2018) 54–68.

[51] X. Wen, T. Zirwes, A. Scholtissek, H. Böttler, F. Zhang, H. Bockhorn, C. Hasse, Flame structure analysis and composition space modeling of thermodiffusively unstable premixed

hydrogen flame — Part II: Elevated pressure, Combust. Flame (2021) submitted.

[52] R. Addabbo, J. Bechtold, M. Matalon, Wrinkling of spherically expanding flames, Proc. Combust. Inst. 29 (2002) 1527–1535.

[53] W. Han, A. Scholtissek, C. Hasse, The role of tangential diffusion in evaluating the performance of flamelet models, Proc. Combust. Inst. 37 (2019) 1767–1774.